This is a preprint, the final version is subject to change, of the American Mineralogist (MSA)
Cite as Authors (Year) Title. American Mineralogist, in press.
(DOI will not work until issue is live.) DOI: http://dx.doi.org/10.2138/am-2016-5407

REVISION 2

Computational study of pressure behaviour to 6 GPa of the $2M_1$ muscovite-paragonite series

N. HERNÁNDEZ-HARO,[1] D. MUÑOZ-SANTIBURCIO,[1,4] C. PÉREZ DEL VALLE,[2] J. ORTEGA-CASTRO,[3] C. I. SAINZ-DÍAZ,[1] C. J. GARRIDO,[1] AND A. HERNÁNDEZ-LAGUNA[1,*]

[1]*Instituto Andaluz de Ciencias de la Tierra (CSIC-UGR), Av. de las Palmeras 4, 18100-Armilla, Granada, Spain.*

[2]*Université Grenoble Alpes, DCM F-38000 Grenoble Cedex 9, France.*

[3]*Departament de Química, Institut d'Investigació en Ciències de la Salut (IUNICS), Universitat de les Illes Balears, E-07122 Palma de Mallorca, Spain.*

[4] *Present address: Lehrstuhl für Theoretische Chemie, Ruhr-Universität Bochum, 44780 Bochum, Germany*

[*] Corresponding author: Alfonso Hernández-Laguna, Instituto Andaluz de Ciencias de la Tierra (CSIC-UGR), Av. de las Palmeras 4, 18100 Armilla, Granada, Spain, Tlph: +34958230000 ext 190211, *ahlaguna@ugr.es; alfonso.hernandez@iact.ugr-csic.es*

Abstract

The muscovite (Ms)-paragonite (Pg) series [$K_{1-x}Na_xAl_2(Si_{4-y}Al_y)O_{10}(OH)_2$] is a group of micas with end members of Ms ($x = 0$, $y \approx 1$) and Pg ($x = 1$, $y \approx 1$). This mineral series is found in the Earth's crust and upper mantle. The series shows a wide immiscibility gap between the end members.

Density Functional Theory (DFT) is used to show the compression in five models of the $2M_1$ polytype Ms-Pg series to 6 GPa. Bulk moduli and cell-parameter moduli were obtained from a least square fitting of pressures and volumes to a third-order Birch-Murnaghan equation of state. Bulk-modulus values of the end members of the series agree with the range of experimental values. Bond lengths and atomic-group geometries were studied as a function of the pressure and composition of the series by determining the moduli. Compression mechanism has been determined.

The excess volumes, V^{ex}, were higher for the Na-rich members than for the K-rich members than the solid solution. V^{ex} follow a Redlich-Kister behaviour. The excess free energy, G^{ex}, was calculated isobarically in a semiempirical way: the DFT excess volume data were calculated in one experimental model (A from Roux and Hovis, 1996) in a Redlich-Kister function. The G^{ex} as a function of the composition of the Ms-Pg join of the A model show two minima with constant composition to 0.75 GPa, evolving to richer end member compositions at greater pressures. Therefore, the solvus should increase the gap of immiscibility at high pressure.

Keywords: Muscovite-paragonite series; DFT calculations; pressure behaviour of atomic groups and crystal geometry; bulk modulus; cell-parameter moduli; bonds and atomic-group moduli; compression mechanism; excess volume; excess free energy.

INTRODUCTION

The muscovite (Ms)–paragonite (Pg) join is a series of dioctahedral phyllosilicates of the true, white-mica group, with Na^+ and K^+ substitutions in the interlayer, with a general formula $[K_{1-x}Na_xAl_2(Si_{4-y}Al_y)O_{10}(OH)_2]$. These minerals, found in the Earth's crust and upper mantle, are among the most common and abundant minerals in metamorphic rocks. Ms ($x = 0$, $y \approx 1$) and Pg ($x = 1$, $y \approx 1$) are the end members of the series where an immiscibility gap exists (Guidotti et al., 1992). Natural samples show minor concentration of cations, which involve sites in the interlayer (Ca^{2+}, Ba^{2+}, Sr^{2+}, etc.), octahedra (Oc/VI) (Mg^{2+}, Fe^{2+}, Fe^{3+}, Ti^{2+}, and Mn^{2+}) and tetrahedra (T/IV) sheets. The effect of cation substitutions in the Oc, T sheets and interlayer on the cell dimensions was studied by Guidotti et al. (1992). The Ms-Pg series has the potential to be a geothermometer and a geobarometer (Guidotti et al., 1994; Blencoe et al., 1994).

Pressure behaviour of Ms was studied by different techniques, revealing a strong anisotropy in the compressional behaviour (Comodi and Zanazzi, 1995). Table 1 presents the values of the bulk modulus of Ms and Pg with different experimental techniques. Bulk-modulus values of Ms are given from 49.0 GPa (Holland and Powell, 1998, 2011) to 61.4 GPa (Faust and Knittle, 1994). These variations in results may be attributed to different samples, such as heterogeneities of composition, techniques, and use of powder or single-crystal samples. In addition, in powder samples subject to high pressure, preferred orientations of crystallites are possible. The bulk modulus of Pg was also studied, showing more rigid values (65.5 GPa, Comodi and Zanazzi, 1997) than Ms.

Ortega-Castro et al. (2010) by means of DFT calculations of Ms with increasing pressure to 6 GPa determined a bulk-modulus value of 60.1 GPa. They studied each atomic group as a function of pressure to yield the compression mechanism. This value is close to that of Faust and Knittle (1994). Teich-McGoldrick et al. (2012), by means of dynamical simulations, obtained a bulk modulus of Ms of 59.8 GPa (0.01 GPa of pressure and T=298 K). They found that the bulk moduli decreased with increasing temperature and increased with increasing pressure, as expected. From DFT-calculated

79 elastic constants, polycrystalline bulk moduli of the series have been found to be
80 slightly larger than the known experimental values (Hernández-Haro et al. 2013).

81 Atomic-group variations as a function of pressure was also studied (Comodi and
82 Zanazzi, 1995, 1997, and Guidotti et al., 2000). The micro-environments crystal-
83 chemical and structural properties evolve as a function of the concentration of one
84 cation in a solid solution, pressure, and temperature and they are related to the
85 thermodynamic properties, stability, and evolution of the minerals. However, most of
86 the experiments use macroscopic and thus heterogeneous samples, giving average
87 values of the inter-atomic geometry and properties of the crystal. The use of crystal
88 models free of order/disorder, average compositional effects, heterogeneity, and
89 different experimental preparations can give values of inter-atomic geometry and
90 properties that could be the key to accounting for the nano- and micro-behaviour, and
91 design of new materials. DFT studies, can offer a detailed explanation for the crystal-
92 chemical behaviour of the solid solutions (Geiger, 2008) without the cited drawbacks of
93 the experimental methods.

94 Owing to the effects of pressure on the stability of Ms-Pg pairs and the K/Na
95 ratios of Na-saturated Ms, practical application of the Ms-Pg solvus thermometry is
96 restricted to equilibrated quasi-binary Ms-Pg pairs at pressures between ca. 0.2 and 0.8
97 GPa (Blencoe et al. 1994). The effect of pressure on the Ms-Pg solvus is manifested by
98 the effect on the excess Gibbs free energy (G^{ex}), which varies with the Margules'
99 coefficients (W_G) of excess volume (V^{ex}) (Ganguly, 2008, and references therein). There
100 are major disparities in the literature for experimental molar excess volume data of the
101 Ms-Pg system, making it difficult to constrain the functional form (quadratic, cubic, etc.
102 polynomial) of V^{ex} (Eugster et al.1972; Blencoe, 1977; Chatterjee, 1974; Flux and
103 Chatterjee, 1986, Chatterjee and Flux, 1986; Chatterjee and Froese, 1975; and
104 Chatterjee and Johannes, 1974). Because natural Ms-Pg micas are unstable below the
105 solvus, experimental work in synthetic and natural micas only constrain the volumes in
106 the compositional ranges near the end members. Furthermore, V^{ex} of Ms-Pg micas are
107 small (commonly < 0.13 J/bar), so minor errors in the experimental molar volume affect
108 significantly the accuracy of the V^{ex}. Phase equilibrium data indicate a larger positive
109 V^{ex} than X-Ray measurements, particularly on micas synthesized at very high pressures
110 (Roux and Hovis, 1996). Because there is no such limitation in theoretical methods, the
111 present study may constrain the functional form of V^{ex} of Ms-Pg micas.

112 We have previously studied the pressure behaviour of Ms (Ortega-Castro et al.,
113 2010) and the elastic properties of the Ms-Pg series (Hernández-Haro et al., 2013) by
114 DFT methods. From the elastic constants, the calculated bulk moduli correspond to the
115 average polycrystalline bulk moduli from a Hill average (Hill, 1952) of the upper and
116 lower Hashin and Shtrikman limits (Hashin and Shtrikman, 1962a and b). In this article,
117 we study the pressure behaviour of the series in a periodic single-crystal model,
118 increasing the pressure sequentially with the following aim: to ascertain theoretically
119 how the crystal structure, geometry of the atomic groups, mixing behaviour, and
120 incompressibility moduli evolve with pressure and composition; and to clarify the
121 influence of pressure on the Ms-Pg solvus.

122

METHODS

Crystal model

Each Ms-Pg series model is defined by the following: $[K_{1-x}Na_xAl_2(Si_3Al)O_{10}(OH)_2]$ (x between 0 and 1). Crystal models used are similar to Hernández-Haro et al. (2013). The models of the $2M_1$ polytypes are monoclinic. Figure 1 shows the model of X_{Na} = Na/(Na+K)= 0.5 (atomic fraction of the mica). In Ms with X_{Na} = 0, cations in both interlayers are K^+ and they are increasingly substituted by Na^+ to produce the five studied compositions of the Ms-Pg series to X_{Na} = 1 for Pg. A supercell of 1x1x2 is used for the $2M_1$ polytype X_{Na} = 0, 0.5, and 1. Interlayer cations with the same atomic number are in opposite sides of the layer in both interlayers for X_{Na} = 0.5 (Fig. 1). Compositions with X_{Na} = 0.25 and 0.75 require a 2x1x2 supercell, with cations of the same atomic number in opposite sides in both interlayers (Hernández-Haro et al. 2013).

Computational methods

The Density Functional Theory (Hohenberg and Kohn 1964; Kohn and Sham 1965) calculations were performed with the SIESTA2.0.2 code (Sánchez-Portal et al. 1997; and Artacho et al. 1999; Soler et al., 2002). Periodic boundary conditions were applied to the crystal cells. The atomic groups and cell parameters were optimized together in the same simulation. Generalized gradient approximation (GGA) with the Perdew-Burke-Ernzerhof (Perdew et al. 1996) (PBE) correlation-exchange functional was used. A mesh cut-off of 500 Ry and 15 and 9 k-points in the Monkhorst Pack grid were found to be adequate to produce rapid convergence in the 84 and 168 atom cells, respectively. Our calculations were performed with numerical atomic orbitals, and double-ζ plus polarization basis sets. Troullier-Martins norm-conserving pseudopotentials (Troullier and Martins 1991) were used. Muscovite-$2M_1$ is monoclinic with a C2/c space group. All calculations were performed by fixing the desired pressure, and then optimizing cell parameters and atomic positions to reach convergence thresholds of forces and stresses (0.005 eV/Å and 0.002 GPa, respectively). The applied pressures ranged from -1 to 6

GPa (negative values are tractions) in increments of 0.25 GPa between -1 and 1 GPa, and 0.5 GPa between 1 and 6 GPa.

The pseudopotentials and basis sets used here were previously optimized for a set of dioctahedral 2:1 phyllosilicates (Ortega-Castro et al. 2008, 2009). In a previous paper, the high-pressure behaviour of Ms was calculated in the local density approximation (LDA) with the Ceperley-Alder exchange-correlation functional (Ceperley and Alder 1980) and the GGA-PBE approach. The results showed that the GGA yielded cell parameters closer to the experimental data than LDA (Ortega-Castro et al. 2010; Hernández-Haro et al. 2013). In addition, White et al. (2009) demonstrated that the GGA functional yielded low energies and accurate geometries in kaolinite. Tunega et al. (2012) analysed the role of dispersion corrections in DFT calculations in talc, pyrophyllite, kaolinite and lizardite, employing different functionals with and without dispersion forces, and found that using the dispersion corrections produced better results, especially for *c* axis values. In those systems, where no cation substitutions were present, the atoms across the interlayer were linked mainly by van der Waals forces, whereas in the mica systems, where cations are present in the interlayer, the most important forces are the Coulomb forces, well described by DFT methods.

Equation of state

The bulk modulus, B_0, at P=0 GPa was calculated by fitting a Birch-Murnhagan (BM) equation of state to volumes and pressures [Birch, 1947, EOSFIT5.2 (Angel, 2000, 2001)].The incompressibility of the cell-parameter linear moduli was also calculated by using a cubic crystal with a cell parameter equal to one of the monoclinic cell parameters, and fitting with the aid of EOSFIT 5.2 code (Angel 2000 and 2001). Most of the B_0 values were calculated from a third-order Birch-Murnaghan equation fitting (BM3).

Solid solutions

In a solid solution, the value of any cell parameter of any member, *i*, of the solution can be expressed with respect to the end members by an ideal mixing law, which, for any cell parameter, is defined by Vegard's law:

$$a_i = \sum_j X_{ij} a_j \quad (1)$$

where X_{ij} is the molar fraction of the *j* end member of the solid solution in any *i* member of solid solution. In our solid solution the numbers of end-members are two. A similar law is given for the volume of the crystal cell:

$$V_i = \sum_j X_{ij} V_j \quad (2)$$

Non-ideality can be expressed by mixing excess terms (Waldbaum and Thompson 1968), which for the case of two components in the solid solution can be written as:

$$\Delta V_i^{ex} = W X_{ij}(1 - X_{ij}) \quad (3a)$$

$$\Delta V_i^{ex} = X_{ij}(1 - X_{ij})[W_1(1 - X_{ij}) + W_2 X_{ij}] \quad (3b)$$

W are the Margules' coefficients, where *W* at Eq. (3a) is considered a symmetric excess mixing term of a regular mixing model. In the Eq. (3b), W_1 and W_2 are asymmetric excess mixing terms (Waldbaum and Thompson 1968, Hernández-Haro et al. 2013) belonging to a subregular mixing model; W_1 is associated with the increasing concentration cation considered in the function, and W_2 is associated with the other cation.

The systematization of the bulk modulus as a function of the substitution-cation in the solid solution is established from Eq. (2) by calculating the derivative with respect to pressure, resulting in (Takahashi et al. 1970):

$$\frac{V_i}{B_{0i}} = \sum_j X_{ij} \frac{V_j}{B_{0j}} \quad (4)$$

where B_{0i} and B_{0j} are the bulk modulus of any member and one of the end members of the solid solution, respectively. This equation can be extrapolated to any modulus of the cell parameters, and to any other bond or atomic group (*u*) of the crystal:

$$\frac{u_i}{B_{u0i}} = \sum_j X_{ij} \frac{u_j}{B_{u0j}} \quad (5)$$

Excess free-energy

The Gibbs free energy of any member, *i*, of a solid solution, at a temperature (T) and pressure (P) is given by (Saxena et al. 1993, Fabrichnaya et al. 2004):

$$\Delta G_i^{mix}(T,P) = \sum_{j=1}^{n} X_{ij}\, G_j(T,P) + RT\left(\sum_{j=1}^{n} X_{ij}\, lnX_{ij}\right) + \Delta G^{ex}(T,P) \quad (6)$$

where n is the number of end members and G_j is the free energy of any end member forming the solid solution in an ideal mixing equation. The second term is the configurational entropy of the solid solution terms, and the last term is the excess free energy.

The excess of free energy is given by a Redlich-Kister approach (Redlich and Kister 1948, Ganguly 2008) by a function:

$$\Delta G^{ex}(T,P) = X_{ij}\left(1 - X_{ij}\right)\left[A + B\left(1 - 2X_{ij}\right) + C\left(1 - 2X_{ij}\right)^2\right] \quad (7)$$

Where the A, B and C coefficients are divided in enthalpy, entropy and volume contributions, such as: $A=A_H+A_sT+A_VP$, and with B and C being coefficients of the same partition. Chatterjee and Flux (1986) and Roux and Hovis (1996) used this equation to study the Ms-Pg system.

Although the free energy and the dependence with temperature of the free energy can be calculated theoretically from zero point energy (ZPE) and thermal effects, the number of atoms of our crystal models requires substantial computational resources. For these reasons, excess free energy is calculated isobarically by a classical and semiempirical approach, adding our computational excess free energy coefficients (Eq. 7) depending on the pressure to the experimental enthalpy and entropy coefficients of Eq. (7).

RESULTS AND DISCUSSION

Crystal structure at room pressure

Cell parameters and volume variation as a function of the Na^+ content was studied in Hernández-Haro et al. (2013). The main results of that study are summarized and used here (Table 2) for consistency and for comparison purposes. Cell parameters *a, b, 0.5csinβ* and volumes in Ms and Pg at a pressure of 0 GPa were in agreement with the experimental and average. Tetrahedral cation-oxygen bond averages (<T-O>) and octahedral aluminium –oxygen linkages averages ($<^{VI}Al^{3+}$ - O>) were in agreement with the experimental values (<1%). Si and Al^{3+} tetrahedra, Al^{3+} octahedra volumes, and the Oc-, T-sheet, and interlayer thicknesses (Table 2) yielded values close to the experimental results. Average distances of interlayer cations with the further (outer) and closer (inner) basal oxygen atoms ($<X\cdots O_{outer/inner}>$, $X = Na^+$ or K^+) were consistent with the experimental data (Table 2). The behaviour of these distances with respect to X_{Na} was approximately linear, decreasing with the Na^+ content. Tetrahedral rotation, α, linearly increased with X_{Na} (Table 2), the average values and slope of $<\alpha>_{Na}$ being higher than $<\alpha>_K$. This effect may be related to the highest charge/radius ratio of Na^+ with respect to K^+, which increases the tetrahedral rotation (Muñoz-Santiburcio et al. 2011).

The calculations were performed at 0 K and 0 GPa without any calculation of ZPE and thermal effects, although the experimental data are from samples at room temperature and pressure. The agreement may be related to error cancellation, owing to the basis set size, pseudopotentials, correlation-exchange functional parameters, and the remaining approximations. Nonetheless, the PBE correlation-exchange functional is a nonempirical GGA functional, which yields reliable results (Goerigk & Grimme, 2011), especially for cell volumes (Kurth et al. 1999).

Crystal structure at high pressure

Ms

The *a* axis values of Ms decrease as a function of pressure, being approximately linear from -1 GPa (Fig. 2a). They are compared with the experimental values in Fig. 2a. The calculated value of the *a* axis incompressibility modulus is 490.6 GPa (Table 3), which is larger than the experimental value of 337.8 GPa (Comodi and Zanazzi, 1995), and 400 GPa (Curetti et al., 2006). In this case, no temperature correction was applied to our value, which could yield smaller values of the modulus of the axis, and possibly be closer to the experimental value. In addition, the minerals of Comodi et al. 2002, Curetti et al. (2006), and Gatta et al. (2010) showed phengitic substitutions that could justify the differences with respect to our values. The value of the *b* axis as a function of pressure is close to the experimental values (Fig. 2a). The calculated incompressibility modulus (413.7 GPa, Table 3) of the *b* axis differs from the experimental values of 295.0 GPa (Comodi and Zanazzi, 1995) and 342 GPa (Curetti et al. 2006).

Values of $0.5csin\beta$ as a function of pressure show a small nonlinear behaviour (Fig. 2b), and values of compressibility show a quasi-parallel behaviour with the experimental values. However, experimental and computational values slightly diverge at high pressures. The incompressibility modulus of $0.5csin\beta$ shows a sharp decrease with respect to the *a* and *b* axes, 79.9 GPa (Table 3), which agree with the experimental value (88.2 GPa, Comodi and Zanazzi, 1995). This sharp decrease is related to the weak Coulomb forces in the interlayer, which soften the incompressibility modulus.

The differences between the calculated incompressibility moduli of *a* and *b* and experimental values may be related to three factors: 1) approximations of the DFT methods; 2) the EoS fitting procedure; and 3) a temperature correction is not applied to these calculated values. The temperature correction would surely soften the moduli, thereby making the computational values closer to the experimental values.

The volume as a function of pressure also agrees with the experimental values (Fig 2b). The calculated bulk modulus shows values of 60.0 GPa and 55.6 GPa (with temperature correction from Comodi et al. 2002), which agree with the range of experimental values (Table 1). The value of the first derivative of the bulk modulus with respect to pressure, B_0', is 7.9 (Table S1), which may be consistent with the experimental value of phengite of 6.97 from Curetti et al. (2006), and Gatta et al. (2010), and 6.9 of Faust and Knittle (1994). The closer values between the bulk moduli and the $0.5csin\beta$ moduli indicate that the *c* cell parameter modulus determines the bulk

modulus. Thus, when pressure is applied to the crystal, the stiffness of the entire structure is dominated by the softest direction of the crystal, and this is where the interlayer is located in the phyllosilicates.

Na-rich Ms

The natural sample with a known experimental bulk modulus has X_{Na} = 0.37 (Comodi and Zanazzi, 1995, 1997), which is between the X_{Na} = 0.25 – 0.5 models. Values of *a* and *b* of the X_{Na} =0.25 member as a function of pressure are in agreement with known experimental values (computational and experimental values of *a*, *b*, *0.5csinβ*, and *volume* are seen in Figures S1a and S1b).

The values of *a* and *b* moduli of X_{Na} =0.25 decrease as a function of the Na^+ content in the series (Table 3). Natural Na-rich Ms shows values (Comodi and Zanazzi, 1995) lower than both calculated values, following the same trend as in Ms (Table 3). An additional softening is expected with a temperature correction. In general, the values of B'_{a0} for X_{Na} = 0.25 and = 0.50 are the lowest of the series (Table S1). The value of *0.5csinβ* modulus increases as a function of the Na^+ content (84.5 and 95.9 GPa, for X_{Na} =0.25 and 0.50, respectively), owing to the smaller interlayer as a consequence of shorter ionic radius of the Na^+, the repulsive forces of the negative charged basal O atoms of both layers becoming greater. The experimental value of the *c* modulus for Na-rich Ms (X_{Na} = 0.37) is 98.9 GPa (Comodi and Zanazzi, 1995), which is close to our results for X_{Na} = 0.5.

Our calculated bulk moduli for X_{Na} is equal to 0.25 and 0.50 (60.3 and 62.7 GPa, respectively). The former is slightly higher than the Ms bulk modulus (Table 3). Both values are higher than the experimental bulk modulus of the Na-rich Ms sample, which is 60 GPa (Table 1 and 3). The temperature corrections (Comodi et al. 2002) yield values smaller than the experimental value (Table 3). Values of B_0' of both models are similar to the value for Ms, indicating a similar variation rate for the resistance to the increasing hydrostatic pressure for this series of minerals (Table S1).

Pg

The values of B_{a0} and B_{b0} for X_{Na} = 0.75 and Pg (X_{Na}=1) are lower than previous models, (Table 3), reaching values of 284.4 and 246.3 GPa, respectively. The 284.4 value agrees with the experimental value of Pg (X_{Na} = 0.88, Comodi and Zanazzi 1997). Values of B'_0 of cell axes are close to the above models but, in general, they are the largest in the series (Table S1). The value of $B_{0.5csin\beta}$ is the largest in the series, reaching 128.4 GPa for Pg. The experimental value (Table 3) is between the values of X_{Na} = 0.75 and Pg. This large resistance of Pg to the compression along [001] may be a consequence of the shortest distances between the layers because of the smallest ionic radius of the full substitutions of K^+ by Na^+.

The bulk moduli of both samples are 65.1 and 65.2 GPa, which are equal to the experimental value of Comodi and Zanazzi (1997). By using a temperature correction (Comodi et al. 2002), these values are approximately 3 GPa lower than the experimental values.

The equilibrium volumes are generally calculated by minimization of the electronic energy, forces and stresses at 0 K. Small errors in the calculated 0 GPa and 0 Kelvin volumes would be magnified when calculating the bulk modulus; if V_0 is overestimated, B_0 is underestimated (Kurth et al. 1999). Nonetheless, we obtained consistent results, and where the errors seem to be larger, as in the cell parameter incompressibility moduli, they affect the bulk moduli minimally.

When the bulk moduli of polycrystalline samples of the series are determined from the computational elastic constants from the average (Hill, 1952) of the upper and lower limits of the Hashin-Shtrikman approach (Hashin and Shtrikman, 1962) different results are found: 68.4 and 68.8 GPa for Ms and Pg, respectively (with a minimum at the middle content of Na^+) (Hernández-Haro et al. 2013). However, when temperature corrections were empirically introduced, values are closer to the experimental results. Variations might be related to the approaches intrinsic to DFT calculations, the Hashin-Shtrikman model (Hashin and Shtrikman 1962) and the Hill average (Hill, 1952).

Compression process

354 *Atomic groups compression*

355 In general, the hydrostatic pressure compresses the entire crystal structure, the
356 bonds, bond angles, atomic groups and polyhedra. Incompressibility moduli of bonds
357 and atomic groups are calculated as the inverse of the compressibility values of the
358 average deformations of bonds and atomic groups and fitted by the least square method
359 to first, second and thrird order polynomia.

360 Our calculated Si/Al – $O_{basal/apical}$ average distances decrease with pressure
361 (average values as a function of pressure are in Figure S2), and have very high
362 incompressibility moduli (Table 4). The Si - O_{apical} bonds are shorter than the Si – O_{basal}
363 bonds. The ^{IV}Al - O bond distances are larger than the Si - O bonds, and the moduli
364 smaller than for Si – O bonds (-33%). Overall, Al - O bonds show a similar behaviour
365 as Si - O bonds. The Si/Al – O bond lengths as a function of pressure were studied by
366 Comodi and Zanazzi (1995, 1997) and Guidotti et al. (2000), who found small negative
367 compressibilities. Positive compressibilities were found in our work with high
368 incompressibility moduli, distinguishing Si/Al – O_{basal} or O_{apical} bonds. It is well known
369 that Si –O bonds are mostly incompressible (Levien and Prewwit, 1981; and Hazen and
370 Finger, 1977) although, in some cases, this is dependent on the pressure range (Ralph
371 and Ghose, 1980; and Hugh-Jones and Angel, 1994). Our high values of
372 incompressibility in the Si/Al – O bonds may be considered the limit where a small
373 compressibility could change from positive to negative values with small changes in the
374 DFT electronic parameters.

375 The calculated <OH> bond distances are around 0.974 Å, which agrees with the
376 experimental values of 0.998 Å (Mookherjee et al. 2002 in a $2M_1$ phengite). They are
377 constants in the Ms-Pg series model (Hernández-Haro et al. 2013). When pressure is
378 applied to the crystal, OH bonds enlarge, and a negative compressibility occurs,
379 decreasing linearly with the Na^+ content from $X_{Na} = 0.25$. The negative compressibility
380 was observed in Ms by vibrational spectroscopy as a "bond softening" (Butler and
381 Frost, 2006). From IR spectra, Williams et al. (2012) found that hydrogen bonding
382 increases with pressure.

383 Volumes of the Si tetrahedra and their trend in the series agree with the
384 experimental values (Table 4). Volumes decline with increasing pressure, whereas the
385 experimental Si tetrahedron volumes show a minor increase for Pg, which is consistent

with the behaviour of Si/Al – O bonds. Volumes of Al^{3+} tetrahedra are larger and incompressibility moduli are smaller than the Si tetrahedra and show the same trend (Table 4).

The tetrahedral-sheet thickness (T-thick) values also agree with the experimental values (Table 4), decreasing with increasing pressure, similar to the experimental results; values of their moduli are higher than the experimental values.

Volumes of the octahedral polyhedra agree with the experimental values in Ms, but, in Pg, calculated volumes are slightly higher than the experimental values (Table 4), which decrease with pressure, in agreement with experimental values. The modulus of the octahedral volumes decreases with the Na^+ content in the series, and they are higher than the experimental values. Octahedral-sheet thickness in Ms shows values similar to the experimental values (Table 4). Calculated incompressibility moduli are larger than the experimental values but they show the same behaviour with increasing Na^+ content. The octahedral-sheet thickness is much more compressible than the tetrahedral sheet.

The α angle increases with pressure. Calculated values at room pressure agree with the experimental observation (Table 2), and α_K values (Fig. 3a) and slopes as a function of X_{Na} are smaller than α_{Na}. When pressure is higher, interlayer cations are introduced into the ring cavity, but because the ionic radius of Na^+ is smaller than K^+, tetrahedra must change their rotation to allow a better fit of the smaller Na^+. Because the K^+ cavities are located near the Na^+ cavities, the former change their tetrahedral rotation as a consequence of the rotation of the latter, and this effect is propagated along the layer, causing a stabilizing/destabilizing effect in the cavities. At high pressures, this effect is magnified because the increasing value of α as a function of pressure, $\alpha_{K/Na}$ show negative compressibility. The incompressibility moduli of both α_K and α_{Na} are negative and decline as a function of the Na^+ content in the series (Fig. 3b, Table 4). This effect is more pronounced in α_K.

The $K^+/Na^+ \cdots O_{outer/inner}$ bond distances yield moduli between 64 and 336 GPa (Table 4). The moduli of $K^+/Na^+ \cdots O_{outer}$ are larger than $K^+/Na^+ \cdots O_{inner}$, and $Na^+ \cdots O_{outer}$ modulus in Pg is the largest. Although the *outer* distances might be expected to be more compressible than the *inner* distances because they are larger, the *inner* O atoms

are more greatly affected by the Coulomb field of interlayer cations than the *outer* O, consequently showing greater compressibility. In general, $Na^{+} \cdots O_{outer/inner}$ shows lower incompressibility moduli than $K^{+} \cdots O_{outer/inner}$, with the exception of $Na \cdots O_{outer}$ of Pg.

The key structural feature in phyllosilicates is the interlayer, which decreases as a function of Na^{+} content (Fig. 3c, Tables 1 and 4), but the slopes of the functions *interlayer thickness=f(X_{Na})* are smaller at increasing pressure. This behaviour is due to the small ionic radius of the Na^{+}, which reduces the interlayer with its increasing of Na content. In the Pg end members the basal O atoms of both layers are sufficiently close and repulsion is larger. Thus the values at different pressures of the interlayer thicknesses are closer together at the Pg side than at the Ms side of Figure 3c.

The interlayer thickness incompressibility moduli are the smallest of the structure and agree with the experimental data (Table 4). In Ms, Williams et al. (2012) found two possible mechanisms of compression in the interlayer, below and above the range of 5-8 GPa. The interlayer-thickness/interlayer-thickness-modulus relationship [Eq. (5)] of the series decreases with X_{Na} (Fig. 3d), and is in agreement with the volume/bulk modulus relationship [Eq. (4)] of the series (Fig. 3e). This behaviour shows asymmetric mixing terms, indicating different mixing behaviour for the Ms and Pg sides of the Ms-Pg join.

There is disagreement between the calculated and experimental moduli of some structural features of the crystal but not with the interlayer moduli, indicating that the key structural feature determining the bulk modulus is the interlayer.

Compression mechanism

This series shows great anisotropy, with the bulk moduli of the *a* and *b* axes being 6.1-2.2 (Ms-Pg) times larger than $B_{0.5csin\beta}$. When pressure is applied, the interlayer decreases substantially, interlayer cations penetrate into the tetrahedral ring cavities, and α changes accordingly. In addition, the $K^{+}/Na^{+} \cdots O_{inner/outer}$ distances decrease (more for $K^{+}/Na^{+} \cdots O_{inner}$ than $K^{+}/Na^{+} \cdots O_{outer}$). In the layer, the Oc sheet compresses to a larger extent than the T sheets, but to a much lesser extent than the interlayer. Pg members of the series show more resistance to hydrostatic pressure than Ms members of the series.

Solid solutions

Excess Volume of the Ms-Pg join

Chatterjee and Flux (1986) and Roux and Hovis (1996) used a Redlich-Kister mixing equation [Eq. (7)] to account for the G^{ex} of micas in the Ms-Pg join. In Eq (7)V^{ex} was reduced to a subregular model [Eq (3b)] because the coefficient dependent on the volume, C_v,was set to 0. Hernández-Haro et al. (2013) showed that the mixing volume of micas in the Ms-Pg join at 0 GPa followed a regular mixing law with small positive mixing terms. Our choice of a regular mixing volume equation instead of a subregular model equation was based on the smaller standard deviations obtained by the quadratic polynomial fitting relative to those obtained by the cubic polynomial. As shown below, the calculated excess volumes of micas in the Ms-Pg join indicate that neither the regular nor the subregular models are appropriate.

The excess volume of mixing on the Ms-Pg join is (Blencoe, 1977):

$$V_{Pi}^{ex} = V_{Pi} - \sum_{j=1}^{2} X_{ij} V_{Pj} \qquad (16)$$

where V_{Pi} are the calculated volumes of any member of the solid solution, V_{Pj} are the volumes of the end members of the Ms-Pg join at the temperature and pressure of interest. For comparison to previous studies, we report the pressure in kbar and X_{ij} is the atomic fraction of K in the mica (V^{ex}-X_K) instead of the Na atomic fraction (V^{ex}-X_{Na}) which we have previously used. V^{ex} is calculated at 0, 2.5, 5.0 7.5 15, 30 and 60 kbar. V^{ex} at 0 and 60 kbar is depicted in Figs. 4a-b (in Figure S3 pressures of 7.5 and 15 kbar are shown). In general, the V^{ex} shows higher values for Na-rich than for K-rich members, and V^{ex} shows relative minima for pressures ≤7.5 kbar, and maxima for pressures ≥15 kbar. The largest V^{ex} for the richest Pg compositions may be related to the highest repulsions between the layers as a consequence of the smallest distances between them, because of the lower ionic radius of Na^+. The minima at the approximate center K^+ concentration at the low pressure Ms-Pg joins may arise from the symmetrical cation configurations imposed in our computational models. This result occurs from a balance of empty space in the K^+ and Na^+ cavities with the models being more consistent with the ideal mixing behaviour than its lower and upper concentration solid

solution members. At high pressure, V^{ex} of the Pg-rich members are the largest in the series.

The high asymmetry indicates that the V^{ex} of the Ms-Pg solid solution could be better fitted to a Redlich-Kister model instead of subregular models, as determined by Blencoe (1977) for the 1*M* and $2M_1$ polytypes, Chatterjee and Froese (1975) for the $2M_1$ polytype for the end members of the solid solution, and Eugster et al. (1972) for the 1*M* polytype. Furthermore, in contrast to previous studies (Chatterjee and Flux 1986; and Roux and Hovis, 1996), the Redlich-Kister fitting of DFT V^{ex} requires $C_V \neq 0$, implying that a fourth degree polynomial is required to account for the variation of V^{ex} on the Ms-Pg join (Fig. 4a and d). However, the limited data points in the V^{ex}–X_K functions do not allow fitting except by a quartic polynomial interpolation of the DFT data. The A_V, B_V and C_V terms in Eq. (7) obtained with this interpolation are given in Table 5. The DFT A_V and B_V values are similar to those reported in previous experimental and thermodynamic studies using the Redlich-Kister model (Chatterjee and Flux 1986; Roux and Hovis, 1996), and those derived from Margules' parameters of the subregular model for 1*M* polytypes (Bencloe, 1977; Chatterjee and Froese, 1975) (cf. Table 5). DFT results show the high asymmetry of V^{ex} and its strong pressure dependence. The V^{ex} data were obtained from the DFT calculations at 0 K, but the volumes at different temperatures were corrected by thermal expansion coefficients (Holland and Powell, 1998). The A_V, B_V and C_V are given in Table 5 at different temperatures (298 - 993 K). A_V and C_V present qualitatively distinct behaviour for low and high pressures (Table 5). In contrast, the B_V does not show any clear systematic variation with pressure and is always the smallest of the three coefficients.

Excess Free energy

Chatterjee and Flux (1986) and Roux and Hovis (1996) computed the G^{ex}, and the corresponding enthalpy, entropy and volume excess coefficients using a Redlich-Kister mixing model [Eq. (7)]. Roux and Hovis (1996) presented four models for the G^{ex}, depending on the number of variables, measurements, and samples introduced in the fitting. In their model A, they included all variables, measurements, and samples. Here, we compute G^{ex} in a semiempirical way, using in Eq. (7) the Roux and Hovis' (1996) coefficients for excess enthalpy and excess entropy and our DFT coefficients for V^{ex}. Figure 5 shows the computed G^{ex} as a function of X_K for the A model of Roux and

Hovis (1996) at constant temperature (693 K) and selected pressures to 60 kbar. The G^{ex}-X_K functions for Model A (Fig. 5) have two minima at all pressures, one for the Pg-rich micas and the other for the Ms-rich micas. These minima are related to the bimodal compositions of the Pg-Ms solvus at different pressures. The maxima between both minima is approximately located at the center-composition phase, increasing their relative values with respect to the minima at increasing pressure. The composition of the minima are nearly constant to 7.5 kbar, and are increasingly displaced towards the end-member components at higher pressures, indicating that the solvus and miscibility gap in the Ms-Pg join widen with increasing pressure. This behaviour is consistent with the observed evolution of the Pg-Ms solvus with pressure (Roux and Hovis, 1996).

The behaviour of the model with our V^{ex} coefficients is similar to the behaviour found by Roux and Hovis' (1996), but giving a quantitative change, especially at high pressure, where more pure phases at high pressure are expected to be produced, widening the gap of immiscibility of the join.

IMPLICATIONS

In this work, we compute for the first time the volume behaviour of this solid solution using an atomistic approach based on first principle computational methods. We demonstrate that this approach predicts accurately the volume and compressional behaviour of the solid solution and compares well with macroscopic experimentally derived parameters. Future work will apply first-principle modelling to more complex solid solutions of white micas, to make possible the study of the behaviour of these material in the Earth's interior with high precision. Results will include the magnitudes of solid solutions, structure, and elasticity as a function of pressure at the atomic level. We further show that macroscopic parameters derived from first principles can be combined with thermodynamic data in a semi-empirical way to better understand the volume behaviour of the solid solution with pressure. This will allow the precise determination of the solvus at high pressure with special applications to subduction zone metamorphism.

539 In this work, the evolution of the solvus has been presented only at one
540 temperature, because the dependence with temperature is obtained from experimental
541 data. However, with less complex systems, where the free energy can be easily
542 calculated, the solvus will be able to be calculated, which opens an important
543 computational field to the study of solid solutions.

544

545

546 **ACKNOWLEDGEMENTS**

547

548 The authors thank Prof. S. Guggenheim for his kind and detailed review of this article.
549 We would also like to thank to the "Centro de Supercomputación de Galicia" (CESGA),
550 and "Centro de Servicios de Informática y Redes de Comunicaciones (CSIRC),
551 Universidad de Granada", for providing the computing time. This work was supported
552 by Spanish MCINN and European FEDER grants CGL2005-02681 CGL2008-
553 02850/BTE, FIS2013-48444-C2-2P, RMN1897 and TRA2009-0205, and by the
554 regional agency 'Junta de Andalucía' for the RNM-264 and -363 PAI-grants.

555

References

Angel R.J. (2000) Equations of state. In R.M. Hazen and R.T. Downs (Eds.), High-pressure and high-temperature crystal chemistry. Reviews in Mineralogy and Geochemistry, 41, 35-60.

Angel, R.J. (2001), http://www.geol.vt.edu/rja/

Artacho, E., Sánchez-Portal, D., Ordejón, P., García, A., and Soler, J.M. (1999) Linear-scaling ab-initio calculations for large and complex systems. Physica Status Solidi (b), 215, 809–817.

Birch, F. (1947) Finite elastic strain of cubic crystal. Physical Review, 71, 809 – 824.

Blencoe, J.G., (1977), Molal volumes of synthetic paragonite-muscovite micas. American Mineralogist, 62, 1200-1215.

Blencoe, J.G., Guidotti, C.V., and Sassi, F.P (1994) The paragonite-muscovite solvus:II. Numerical geothermometers for natural, quasibinary paragonite-muscovite pairs. Geochimica et Cosmochimica Acta, 58, 2277-2288.

Brigatti, M.F., Frigieri, P., and Poppi, L. (1998) Crystal chemistry of Mg-, Fe-bearing muscovites-2M_1. American Mineralogist, 83, 775–785.

Burnham, C.W. and Radoslovich, E.W. (1964) Crystal structure of coexisting muscovite and paragonite. Carnegie Institute of Washington Year Books 63, 232-236.

Butler, I.S. and Frost, R.L. (2006) An overview of the high-pressure vibrational spectra of clays and related minerals. Applied Spectroscopy Reviews, 41, 449-471.

586 Catti, M., Ferraris, G., and Ivaldi, G. (1989) Thermal strain analysis in the crystal
587 structure of muscovite $2M_1$ at 700 ºC. European Journal of Mineralogy, 1, 625-632.

588

589 Catti, M, Ferraris, G., Hull, S., and Pavese, A. (1994) Powder neutron diffraction study
590 of $2M_1$ muscovite at room pressure and at 2 GPa. European Journal of Mineralogy, 6,
591 171-178.

592

593 Ceperley, D.M., and Alder, B.J. (1980) Ground state of the electron gas by a stochastic
594 method. Physical Review Letters, 45, 566–569.

595

596 Chatterjee, N.D., (1974) X-ray powder pattern and molar volume of synthetic 2*M*-
597 paragonite refinement. Contributions to Mineralogy and Petrology, 43, 25-28.

598

599 Chatterjee, N.D., and Flux, S. (1986) Thermodynamic mixing properties of muscovite-
600 paragonite crystalline solutions at high temperatures and pressures, and their geological
601 applications. Journal of Petrology, 27, 677-693.

602

603 Chatterjee, N.D., and Froese, E. (1975) Themodynamic study of pseudobinary join
604 muscovite-paragonite in system $KAlSi_3O_8$-$NaAlSi_3O_8$-Al_2O_3-SiO_2-H_2O. American
605 Mineralogist, 60, 985-993.

606

607 Chatterjee, N.D. and Johannes, W. (1974) Thermal stability and standard
608 thermodynamics properties of synthetic $2M_1$ Muscovite, $KAl_2[AlSi_3O_{10}(OH)_2]$.
609 Contributions to Mineralogy and Petrology, 48, 80-114.

610

611 Comodi, P., and Zanazzi, P.F. (1995) High-pressure structural study of muscovite.
612 Physics and Chemistry of Minerals, 22, 170–177.

613

614 - (1997) Pressure dependence of structural parameters of paragonite. Physics and
615 Chemistry of Minerals, 24, 274-280.
616

Comodi, P., Gatta, G.D., Zanazzi, P.F., Levy, D., and Crichton, W. (2002) Thermal equations of state of dioctahedral micas on the join muscovite-paragonite. Physics and Chemistry of Minerals, 29, 538–544.

Curetti, N., Levy, D., Pavese, A., and Ivaldi, G. (2006) Elastic properties and stability of coexisting 3T and 2M_1 phengite polytipes. Physics and Chemistry of Minerals, 32, 670–678.

Eugster, H.P., Waldbaum, D.R., Thompson, J.B., Bence, A.E., and Albee, A.L. (1972) The two-Phase region and excess mixing properties of paragonite-muscovite crystalline solutions. Journal of Petrology, 13, 147-179.

Fabrichnaya, O., Saxena, S.K., Richet, P., and Westrum, E.F. (Eds.) (2004) Thermodynamics data, models, and phase diagrams in multicomponets oxide systems. Springer-Verlag, Berlin.

Faust, J., and Knittle, E. (1994) The equation of state, amorphization and high pressure phase diagram of muscovite. Journal of Geophysical Research, 99, 19785–19792.

Flux, S., and Chatterjee, N.D. (1986) Experimental reversal of the Na-K exchange reaction between muscovite-paragonite crystalline solutions and a 2 molal aqueous (Na,K)Cl fluid. Journal of Petrology, 27, 665-676.

Ganguly, J. (2008) Thermodynamics in Earth and Planetary Sciences. Heidelberg, Springer.

Gatta, G.D., Rotiroti, N., Lotti, P., Pavese, A., and Curetti, N. (2010) Structural evolution of a 2M_1 phengite mica up to 11 Gpa: in situ single crystal X-ray diffraction study. Physics and Chemistry of Minerals, 37, 581-591.

Geiger, C. A. (2008) Silicate garnet: A micro to macroscopic (re)view. American Mineralogist, 93, 360 -372.

649

650 Goerigk, L. and Grimme, S. (2011) A thorough benchmark of density functional
651 methods for general main group thermochemistry, kinetics, and noncovalent
652 interactions. Physics Chemical Chemical Physics, 13, 6670-6688.
653

654 Guggenheim, S., Chang, Y.-H., and Koster van Groos, A.F. (1987) Muscovite
655 dehydroxylation: High-temperature studies. American Mineralogist, 72, 537-550.

656

657 Guidotti C.V., Mazzoli C., Sassi F.P., and Blencoe, J.G. (1992) Compositional controls
658 on the cell dimensions of $2M_1$ muscovite and paragonite. European Journal of
659 Mineralogy, 4, 283-297.

660

661 Guidotti, C.V., Sassi F.P., Blencoe, J.G., and Selverstone, J. (1994) The paragonite-
662 muscovite solvus:I. P-T-X limits derived from the Na-K compositions of natural,
663 quasibinary paragonite-muscovite pairs. Geochimica et Cosmochimica Acta, 58, 2269-
664 2275.

665

666 Guidotti, C.V., Sassi, F.P., Comodi, P., Zazzi, P.F. and Blencoe, G. (2000) The
667 contrasting responses of muscovite and paragonite to increasing pressure: petrological
668 implications. The Canadian Mineralogist, 38, 707 – 712.

669

670 Hazen, R.M. and Finger, L.W. (1977) Compressibility and structure of Angra dos Reiss
671 fassaite. Carnegie Institution of Washington Year Book, 76, 512-515.

672

673 Hashin, Z., and Shtrikman, S. (1962a) On some variational principles in anisotropic and
674 non-homogeneus elasticity. Journal of Mechanical Physics of Solids, 10, 335–342.

675

676 - (1962b) A variational approach to the theory of the elastic behaviour of
677 polycrystals. Journal of Mechanical Physics of Solids, 10, 343 – 352.

678

679 Hill, R. (1952) The elastic behaviour of a crystalline aggregate. Proceedings of the
680 Physical Society of London A, 65, 349-354.

681

Hernández-Haro, N., Ortega-Castro, J., Pérez del Valle, C., Muñoz-Santiburcio, D., Sainz-Díaz, C.I., and Hernández-Laguna, A. (2013) Computational study of the elastic behaviour of the $2M_1$ muscovite-paragonite series. American Mineralogist, 86, 651 - 664.

Hohenberg, P., and Kohn, W. (1964) Inhomogeneous electron gas. Physical Review B, 136, 864–871.

Holland, T.J.B., and Powell, R. (1998) An internally consistent thermodynamic data set for phases of petrological interest. Journal of Metamorphic Geology, 16, 309 – 343.

- (2011) An improved and extended internally consistent thermodynamic dataset for phases of petrological interest, involving a new equation of state for solids. Journal of Metamorphic Geology, 29, 333-383.

Hugh-Jones, D.A., and Angel, R.J. (1994) A compressional study of $MgSiO_3$ orthoenstatite up to 8.5 GPa. American Mineralogist, 79, 405-410.

Kohn, W., and Sham, L.J. (1965) Self-consistent equations including exchange and correlation effects. Physical Review, 140, A1133–A1138.

Kurht S., Perdew, J.P. and Blaha, P. (1999) Molecular and solid state tests of density functionals approximations: LSD, GGAs, and Meta-GGAs. International Journal of Quantum Chemistry, 75, 889-909.

Levien, L., and Prewitt, C.T. (1981) High-pressure study of diopside, American Mineralogist, 66, 315-323.

Lin, C.Y., and Bailey, S.W. (1984) The crystal Structure of Paragonite $2M_1$. American Mineralogist, 69, 122–127.

Mookherjee, M., Redfern, S.A.T., and Zhang, M. (2001) Thermal response of structure and hydroxyl ion of phengite-2M_1: an in situ neutron diffraction and FTIR study. European Journal of Mineralogy, 13, 545 – 555.

Mookherjee, M., and Redfern, S.A.T. (2002) A high-temperature Fourier transform infrared study of the interlayer and Si-O-stretching region in phengite-2M_1. Clay Minerals, 37, 323-336.

Muñoz-Santiburcio, D., Ortega-Castro, J., Huertas, F.J. , and Hernández-Laguna, A. (2011) Influence of the exchangeable cation on the adsorption of 2-nitro-1-propanol on smectite surface models. Chemical Physics Letters, 515, 49–55.

Ortega-Castro, J., Hernández-Haro, N., Hernández-Laguna, A., and Sainz-Díaz, C.I. (2008) DFT calculation of crystallographic properties dioctahedral 2:1 phyllosilicates. Clay Minerals, 43, 351–361.

Ortega-Castro, J., Hernández-Haro, N., Muñoz-Santiburcio, D., Hernández-Laguna, A., and Sainz-Díaz, C.I. (2009) Crystal structure and hydroxyl group vibrational frequencies of phyllosilicates by DFT methods. Journal of Molecular Structure THEOCHEM, 912, 82–87, DOI:10.1016/j.theochem.2009.02.013.

Ortega-Castro, J., Hernández-Haro, N., Timón, V., Sainz-Díaz, C.I. and Hernández-Laguna, A. (2010) High-pressure behaviour of 2M_1 Muscovite. American Mineralogist, 95, 249–259. DOI: 10.2138/am.2010.3035.

Perdew, J.P., Burke, K., and Ernzerhof, M. (1996) Generalized gradient approximation made simple. Physical Review Letters, 77, 3865–3868.

Prencipe, M., Scanavino, I, Nestola, F., Merlini, M. Civalleri, B., Bruno, M., and Dovesi, R. (2011) High-pressure thermos-elastic properties of beryl ($Al_4Be_6Si_{12}O_{36}$) from *ab initio* calculations, and observations about the source of thermal expansion. Physics and Chemistry of Minerals, 38, 223-239.

Ralph, R.L., and Ghose, S. (1980) Enstatite, $Mg_2Si_2O_6$: Compressibility and crystal structure at 21 kbar (abs.). EoS, 61, 409.

Redlich, O., and Kister, T. (1948) Algebraic representation of thermodynamic properties and the classification of solutions. Industrial and Engineering Chemistry, 40, 345-348.

Rothbauer, R. (1971) Untersuchung eines $2M_1$-muskovits mit neutronenstrahlen, Neues Jahrbuch für Mineralogie Monatshefte, 1971, 143-154.

Ruox, J., and Hovis, G.L. (1996) Thermodynamic mixing model for muscovite-paragonite solutions based on solutions calorimetric and phase equilibrium data. Journal of Petrology, 57, 1241-1254.

Sánchez-Portal, D., Ordejón, P., Artacho, E., and Soler, J.M. (1997) Density-functional method for very large systems with LCAO basis sets. International Journal of Quantum Chemistry, 65, 453–461.

Saxena, S.K., Chatterjee, N., Fei, Y., and Shen, G. (1993) Thermodynamic data on Oxides and silicates. Springer-Verlag, Berlin.

Sekine, T., Rubin, A.M., and Ahrens, T.J. (1991) Shock wave equation of state of muscovite. Journal of Geophysical Research, 96, 19675–19680.

Smyth, J.R., Jacobsen, S.D., Swope, R.J., Angel, R.J., Arlt, T., Domanik, K., and Holloway, R. (2000) Crystal structures and compressibilities of synthetic $2M_1$ and $3T$ phengite micas. European Journal of Mineralogy, 12, 955-963.

Soler, J.M., Artacho, E., Gale, J.D., García, A., Junquera, J., Ordejón, P., and Sánchez-Portal, D. (2002) The SIESTA method for ab-initio order-N materials simulation. Journal of Physics: Condensed Matter, 14, 2745-2779.

778 Takahashi, T., and Liu, L. (1970) Compression of ferromagnesian garnets and the effect
779 of solid solutions on the bulk modulus. Journal of Geophysical Research, 75, 5757-
780 5766.

781

782 Teich-McGoldrick, S.L., Greathouse, J.A., and Cygan R.T. (2012) Molecular dynamic
783 simulations of structural and mechanical properties of muscovite: pressure and
784 temperature effects. Journal of Physical Chemistry C, 116, 15099-15107.

785

786 Troullier, N., and Martins, J.L. (1991) Efficient pseudopotentials for plane-wave
787 calculations. Physical Review B, 43, 1993–2006.

788

789 Tunega, D., Bučo, T., and Zaoui, A. (2012) Assessment of ten DFT methods in
790 predicting structures of sheet silicates: Importance of dispersion corrections. Journal of
791 Chemical Physics, 137, 114105.

792

793 Vaughan, M.T., and Guggenheim, S. (1986) Elasticity of muscovite and its relationship
794 to crystal structure. Journal of Geophysics Research, 91, 4657-4664.

795

796 Waldbaum, D.R., and Thomson, J.B. (Jr.) (1968) Mixing properties of sanidine
797 crystalline solutions. II Calculation based volume data. American Mineralogist, 53,
798 2000- 2017.

799

800 White, C.E., Provis, J.L., Riley, D.P., Kearley, G.J., and van Deventer, J.S.J. (2009)
801 What is the structure of Kaolinite? Reconciling Theory and Experiment. Journal of
802 Physical Chemistry B, 113, 6756-6765.

803

804 Williams, Q., Knittle, E., Scott, H.P., and Liu, Z. (2012) The high-pressure behavior of
805 micas: Vibrational spectra of muscovite, biotite, and phlogopite to 30 GPa. American
806 Mineralogist, 97, 241–252.

807

Captions for the figures

Figure 1.- Crystal structure of the X_{Na} = 0.5 model of the Ms – Pg series. Sky- and navy-blue polyhedrons represent the Al^{3+} and Si^{4+} cation polyhedrons, respectively; the O, H, Na, and K atoms are represented by red, white, yellow, and purple spheres, respectively.

Figure 2.- (a) and (c) variation of *a* and *b* [, (b) and (d) *0.5csinβ* (Å) (0.5csinbe or 0.5csb in the insets) and *volume* (*V*, $Å^3$) of Ms and Pg, respectively, as a function of pressure. In the insets: *j*CZ1995 means values of parameter *j* from Comodi and Zanazzi (1995); *j*298Co2002 means values at 298K from Comodi et al. (2002); *j*Gat2010 means from Gatta et al. (2010); and *j*20MRZ2001 means values at 20 ºC from Mookherjee et al. (2001); where *j* is either *a*, *b*, *0.5csinbe/0.5csb* or *volume* (*Vol)*.

Figure 3.- (a) tetrahedral rotation (α, in degrees) in the Na^+ and K^+ cavities at 0, 3, and 6 GPa; (b) incompressibility modulus×(-1) (GPa) of tetrahedral rotation, α, in the Na^+ and K^+ cavities; (c) interlayer thickness (Å) at 0, 3, and 6 GPa; (d) Interlayer thickness/interlayer thickness modulus (Å/GPa); and (e) volume/bulk modulus ($Å^3$/GPa) as a function of Na^+ content in the series. Insets: least-square fitting equations, correlation coefficients (R or R^2), standard deviations (SD), and Margules' coefficients (W_i).

Figure 4.- Excess volume V^{ex} (J/bar) at different pressures. (a) 0, and (b) 60 kbar as a function of X_K. Values in the insets are from interpolated quadratic polynomial, and A_V, B_V and C_V are the coefficients of Eq. (7) for the V^{ex}, at 298 K. Volumes have been corrected as a function of temperature (Holland and Powell, 1998).

Figure 5.- Excess free energy G^{ex} (KJ/mol) at different pressures. Coefficients of enthalpy and entropy of Eq. (7) was taken from the Model A of Roux and Hovis (1996). Model A is calculated at 693 K.

Captions for the supplementary material figures

Figure S1.- (a) variation of *a* and *b*, (b) *0.5csinβ* (Å) (0.5csinbe or 0.5csb in the insets) and *volume* (*V* or *Vol*, Å^3), of X_{Na} = 0.25 (Na-Ms), respectively, as a function of pressure. In the insets: *j*CZ1995 means values of parameter *j* from Comodi and Zanazzi (1995); where *j* is either *a*, *b*, *0.5csinbe/0.5csb* or *volume*.

Figure S2.- Variation of Si/^{IV}Al – $O_{b(basal)/a(apical)}$ average distances (Å) as a function of pressure (GPa). Ms/Pg/NaMsT*i*OCZ95/97 mean tetrahedral cation O bond (T*i*-O) distances from Ms, Pg or Na-rich Ms from Comodi and Zanazzi (1995) or (1997), where *i* means site 1 or 2.

Figure S3.- Excess volume V^{ex} (J/bar) at different pressures as a function of X_K . (a) 7.5 kbar, and (b) 15 kbar. Values in the insets are from interpolated quadratic polynomial, and A_V, B_V and C_V are the coefficients of Eq. (7) for the V^{ex}, at 298 K. Volumes have been corrected as a function of temperature (Holland and Powell, 1998).

Table 1.- Bulk modulus (B_0 in GPa) and their derivatives with respect to pressure [B_0', B_0'' (GPa^{-1}) first and second derivative of B_0 with respect to pressure in brackets] values for Ms and Pg from different experimental and computational studies.

Ref.	Ms	Pg
Vaughan et al. (1986)	58.2[a]	
Sekine et al. (1991)	52[b] (3.2)	
Faust and Knittle(1994)	61.4[cd] (6.9)	
Catti et al. (1994)	56[e] (4)	
Comodi & Zanazzi (1995, 1997)	56.0[c,f], 60.0[c,f,g]	65.5[c,f,h]
Smyth et al., (2000) Phengite	57[c] (9.2)	
Comodi et al. (2002)	57.0[c,d]	59.9[c,d]
Curetti et al. (2006), Phengite	57.3[c,d] (6.97)	
Gatta et al. (2010) Phengite	57.3[c,f] (6.97)	
Ortega-Castro et al. (2010)	60.1[i] (7.3) , 55.7[j]	
Holland & Powell (2011)	49.0 (4.15,-0.085)	51.5 (6.51, -0.126)
Teich-McGoldrick et al. (2012)	59.8[k]	
Hernández-Haro et al. (2013)	68.4[l], 64.0[j]	68.8[l], 65.5[j]

[a] Brillouin scattering.

[b] Shock wave.

[c] X-Ray diffraction.

[d] Neutron diffraction.

[e] Powdered sample.

[f] Monocrystal sample.

[g] Na-rich Ms, Na 0.37 per formula unit (pfu).

[h] Na 0.88 pfu.

[i] DFT.

[j] An estimate of the bulk modulus at 298 K from Comodi et al. (2002).

[k] Molecular dynamics simulations.

[l] DFT and Hashin-Shtrikman (1962)-Hill (1952) approaches.

This is a preprint, the final version is subject to change, of the American Mineralogist (MSA)
Cite as Authors (Year) Title. American Mineralogist, in press.
(DOI will not work until issue is live.) DOI: http://dx.doi.org/10.2138/am-2016-5407

Table 2. Calculated and experimental structural parameters of Ms-Pg series (lengths in Å, angles in degrees, and volumes in Å^3). X_{Na} =Na^+/(Na^++K^+).

Parameter[a]	Experimental[b]	Experimental[c]	X_{Na} =0.0	0.25	0.5	0.75	1.0
a	5.174-5.226	5.128-5.135	5.187	5.176	5.160	5.152	5.123
b	8.976-9.074	8.898-8.906	9.006	8.994	8.975	8.932	8.895
c	19.875-20.097	19.287-19.384	20.148	19.917	19.653	19.378	19.113
β	95.59-95.84	94.35-94.6	95.44	95.55	95.55	94.08	94.02
Volume	926-945.4	877.51-883.6	936.999	922.829	906.007	889.581	868.767
T-O	1.64	1.653	1.651, 1.757	1.649,1.758	1.675,1.761	1.653, 1.763	1.655, 1.766
M-O	1.927-1.94	1.908-2.221	1.934	1.922	1.931	1.920	1.926
M-OH	1.911	1.896	1.918	1.918	1.912	1.911	1.903
$K\cdots O_{outer}$	3.272-3.373	-	3.427	3.402	3.384	3.372	-
$K\cdots O_{inner}$	2.832-2.934	-	2.759	2.721	2.680	2.624	-
Δ_K	0.426-0.509	-	0.668	0.681	0.704	0.748	-

$Na\cdots O_{outer}$	-	3.370-3.374	-	3.438	3.407	3.352	3.357
$Na\cdots O_{inner}$	-	2.624-2.642	-	2.680	2.618	2.514	2.474
Δ_{Na}	-	0.746-0.732	-	0.758	0.789	0.838	0.883
Tetrahedral rotation α_K, α_{Na}(º)	10.3 [d]- 11.3	16,16.2 - 19	14.6	15.1, 15.8	15.5 , 16.7	16.5, 17.5	18.8
V(T) Si,Al (Å^3)		2.32	2.273, 2.774	2.274, 2.784	2.282, 2.794	2.283, 2.810	2.298, 2.824
V(Oc) Al (Å^3)		9.10	9.386	9.361	9.345	9.339	9.283
Tetrahedral-sheet thickness (Å)	2.262 [d]	2.243	2.277	2.265	2.271	2.248	2.237
Octahedral-sheet thickness (Å)	2.083 [d]	2.078-2.085	2.093	2.090	2.089	2.115	2.144
Interlayer thickness (Å)	3.375 [d]	3.053-3.090	3.361	3.273	3.128	3.021	2.867

[a] V(T) means volume of the tetrahedral sheet, V(Oc) is the volume of octahedral sheet; $\tau = O_{basal}$-T-O_{apical} bond angles ; Tetrahedral rotation α (º) = ½ $\Sigma_{i=1,6}$ [120º - $(O_b$-O_b-$O_b)_i$]/6; Tetrahedral-sheet thickness (Å) = [(mean z coordinate of the "upper" basal O) – (mean z coordinate of the "lower"apical O)]*csinβ*; octahedral-sheet thickness (Å) = [(mean z coordinate of "upper" O or OH in the octahedral sheet) – (mean z coordinate of "lower" O or OH in the octahedral sheet)]*csinβ*.

[b] Burnham and Radoslovish (1964) $K_{0.66}Na_{0.34}Al_2(AlSi_3)O_{10}(OH)_2$; Rothbauer (1971) $K_{0.85}Na_{0.1}(Al_{1.81}Fe^{2+}_{0.14}Mg_{0.12})(Al_{0.9}Si_{3.1})O_{9.8}(OH)_2$; Guggenheim et al. (1987) $K_{0.93}Na_{0.08}(Al_{1.83}Fe_{0.16}Mg_{0.01})(Al_{0.90}Si_{3.10})O_{10}(OH)_{1.83}F_{0.17}$ and $K_{1.00}Na_{0.03}Ca_{0.01}(Al_{1.93}Fe_{0.01}Mn_{0.01})(Al_{0.91}Si_{3.09})O_{10}(OH)_{1.88}F_{0.12}$; Catti et al. (1989) $K_{0.86}Na_{0.11}(Al_{1.93}Fe_{0.07}Mg_{0.02})(Al_{0.92}Si_{3.08})O_{10}(OH)_2$; Catti et al. (1994) $K_{0.90}Na_{0.07}(Al_{1.63}Fe_{0.23}Mg_{0.16}Ti_{0.03})(Al_{0.80}Si_{3.20})O_{10}(OH)_2$; Guidotti et al. (1992); Brigatti et al. (1998) Different compositions; Mookherjee and Redfern (2002) $K_{0.95}Na_{0.05}(Al_{0.76}Fe_{0.14}Mg_{0.10})_2(Al_{0.75}Si_{3.25})O_{10}(OH_{1.96}F_{0.04})$

[c] Comodi and Zanazzi (1997) $Na_{0.88}K_{0.10}Ca_{0.01}Ba_{0.01}(Al_{1.97}Ti_{0.007}Fe_{0.01}Mn_{0.006})Si_{3.01}Al_{0.99}O_{10}(OH)_2$: Guidotti et al. (1992); Lin & Baley, (1984) $K_{0.042}Na_{0.916}Ca_{0.018}\square_{0.024}(Al_{1.990}Fe_{0.028}Mg_{0.013}Ti_{0.003})(Al_{1.061}Si_{2.939})O_{10}(OH)_2$

[d] Comodi and Zanazzi (1995) $K_{0.9}Na_{0.07}Ba_{0.01}\square_{0.02}(Al_{1.84}Ti_{0.04}Fe_{0.07}Mg_{0.04})(Al_{0.98}Si_{3.02})O_{10}(OH)_2$

Table 3.- Bulk moduli (B_0 in GPa) and cell parameter moduli (B_a, B_b, and $B_{0.5csin\beta}$ in GPa) at 0 and 6 Gpa of the Ms-Pg series. Temperature correction for bulk moduli comes from Comodi et al. (2002), considering, in an initial approach, linearity from 0K.

		x = 0.0	x = 0.25	x = 0.5	x = 0.75	x = 1.0
B_a	*(0 GPa)*	490.6	444.9	369.8	324.6	284.4
	(6 GPa)	526.0	452.7	386.0	356.4	319.84
	(exp)	337.8[a], 400[b]		342.5[c]		285.7[d]
B_b	*(0 GPa)*	413.7[e]	365.8	322.1	276.5	246.3
	(6 GPa)	437.7	385.0	349.1	304.7	284.1
	(exp)	295.0[a], 342[b]		287.3[c]		277.8[d]
$B_{0.5csin\beta}$	*(0 GPa)*	79.9	84.5	95.9	115.8	128.4
	(6 GPa)	111.7	122.9	137.9	151.2	166.8
	(exp)	88.2[a],86.9[b,f]		98.9[c,f]		120.4[d,f]
B_0	*(0 GPa)*	60.0	60.3	62.7	65.1	65.2
	(0 GPa, 298K)	55.6	56.2	58.9	61.6	62.0
B	*(6 GPa)*	93.8	94.4	97.1	97.5	98.2
	(6 GPa, 298K)	103.12	105.3	106.1	101.1	103.6
B_0	*(exp)*	56.0[a,d]		60.0[c,d]		65.0[d]

[a] From $K_{0.9}Na_{0.05}Ba_{0.01\ \ 0.02}(Al_{1.84}Ti_{0.04}Fe_{0.07}Mg_{0.04})(Si_{3.02}Al_{0.98})O_{10}(OH)_2$ Comodi and Zanazzi (1995)

[b] From $K_{0.98}Na_{0.02}(Al_{1.55}Mg_{0.24}Fe_{0.21}Ti_{0.02})(Si_{3.38}Al_{0.62})O_{10}(OH)_2$ Curetti et al. (2006).

[c] From $K_{0.6}Na_{0.37\ \ 0.03}(Al_{1.84}Ti_{0.02}Fe_{0.10}Mg_{0.06})(Si_{3.03}Al_{0.97})O_{10}(OH)_2$ Comodi and Zanazzi (1995)

[d] From $K_{0.10}Na_{0.88}Ca_{0.01}Ba_{0.01}(Al_{1.97}Ti_{0.007}Fe_{0.01}Mn_{0.002}Mg_{0.006})(Si_{3.01}Al_{0.99})O_{10}(OH)_2$ Comodi and Zanazzi (1997)

[e] Birch-Murnagham second-order equation

[f] *c* axe.

Table 4.- Values of average (<*i*>) bond distances (Å), volumes (Å^3) tetrahedral distortion angle (α º), and atomic groups at a pressure of 0 and 6 GPa, incompressibility moduli of the average variable (<*i*>) (GPa) of Ms (Mod. Ms) and Pg (Mod. Pg); a and b subindexes under O mean apical and basal oxygens, respectively.

Group	Ms $<i>_{0,6}$		Pg $<i>_{0,6}$		Mod. Ms	Mod. Pg
	0 GPa	6 GPa	0 GPa	6 GPa		
Si-O_b	1.653, 1.640		1.659, 1.651		775.2	1802.8
Si-O_a	1.646, 1.637		1.647, 1.639		1173.7	1000.0
^{IV}Al-O_b	1.754, 1.737		1.768, 1.754		520.8	751.9
^{IV}Al-O_a	1.763, 1.750		1.760, 1.748		781.2	925.9
T – O exp	1.646, 1.64[a]		1.652, 1.66[b]			
K···O_{inner}	2.760, 2.611		2.680, 2.551[c]		74.8	88.3[c]
K···O_{outer}	3.442, 3.356		3.310, 3.256[c]		156.2	290.0[c]
Na···O_{inner}	2.706, 2.535[d]		2.535, 2.370		64[d]	64.7
Na···O_{outer}	3.395, 3.282[d]		3.412, 3.370		109[d]	336.7
V(Td)Si[e]	2.273, 2.221		2.297, 2.265		262	463
V(T)Si V(T)Si exp	2.28, 2.27[a]		2.31, 2.35[b]			
V(T)Al[e]	2.774, 2.697		2.824, 2.760		210.1	267.4
V(Oc)[e]	9.388, 9.212		9.283, 9.065		318	224
V(Oc) exp	9.31,9.04[a]		9.10, 8.6[b]		105[f]	65.9[f]
α_K	14.6, 15.2		16.5, 18.4[c]		- 92	- 40[c]
α_{Na}	15.8, 17.6[d]		18.9, 21.3		- 47[d]	- 33.5
T-thick[e]	2.277, 2.262[a]		2.237, 2.226[b]		917	1828.1
T-thick exp	2.262, 2.237		2.243, 2.25		249	
Oc-thick[e]	2.093, 2.069		2.144, 2.107		483	248.7
Oc-thick exp	2.083, 2.047[a]		2.085, 1.98[b]		159[f]	78[f]
Interlayer-thick[e]	3.361, 2.954		2.867, 2.632		32	51.1
Interlayer-thick exp	3.375, 3.128[a]		3.090, 2.81[b]		37.6[f]	44.7[f]

[a] Ms at 0.0001 and 2.8 GPa, Comodi and Zanazzi (1995)

[b] Pg at 0.0001 and 4.05 GPa, Comodi and Zanazzi (1997)

[c] Values $X_{Na} = 0.75$

[d] Values $X_{Na} = 0.25$

[e] V(T)Si/Al = Volume of the Si/Al tetrahedra, V(Oc) = Volume of the octahedral, T/Oc-thick = Tetrahedral/Octahedral-sheet thickness, Interlayer-thick = Interlayer thickness

[f] Incompressibility modulis estimated from the values of Comodi and Zanazzi (1995) and (1997)

Table 5.- A_V, B_V and C_V coefficients (J/bar) of Eq. (7) at different pressures (kbar) and temperatures (K).

Mod	P (kbar)	T (K)	A_V	B_V	C_V
B[a]	8	677-943	0.2760	-0.0372	-
C&Fr[b]	1-7	848-1008	0.1044	-0.5606	-
C&F[c]	5-7	723-893	0.2359	-0.084	-
A (R&H)[d]	1.0-9.0	853-973	0.350	0.037	-
This work[e]	0.0	298	0.190	0.070	0.315
“	0.0	693	0.196	0.071	0.320
“	0.0	793	0.198	0.072	0.322
“	0.0	893	0.200	0.072	0.323
“	0.0	993	0.202	0.073	0.325
“	2.5	298	0.181	0.050	0.390
“	5.0	298	0.192	0.056	0.390
“	7.5	298	0.188	0.047	0.332
“	15.0	298	0.217	0.119	0.139
“	30.0	298	0.226	0.092	0.161
“	60.0	298	0.213	0.065	0.079

[a] Blencoe (1977), from his Margules’ coefficients.

[b] Chatterjee and Froese (1975), from their Margules’ coefficients.

[c] Chatterjee and Flux (1986).

[d] Model A of Roux and Hovis (1996).

[e] Volumes have been corrected as a function of temperature (Holland and Powell, 1998).

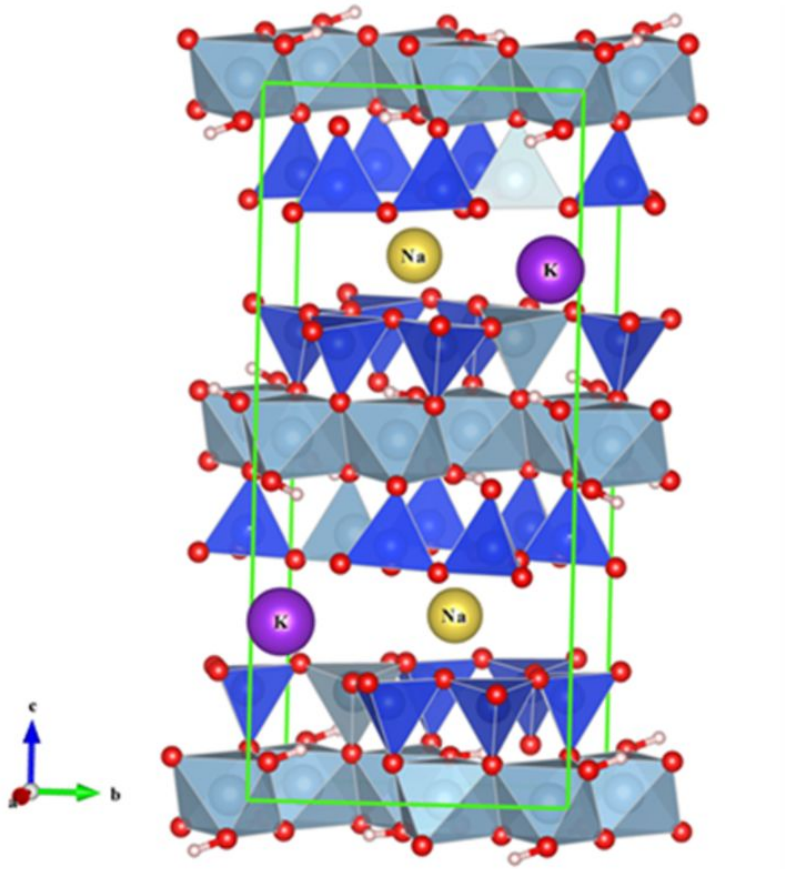

Figure 1

This is a preprint, the final version is subject to change, of the American Mineralogist (MSA)
Cite as Authors (Year) Title. American Mineralogist, in press.
(DOI will not work until issue is live.) DOI: http://dx.doi.org/10.2138/am-2016-5407

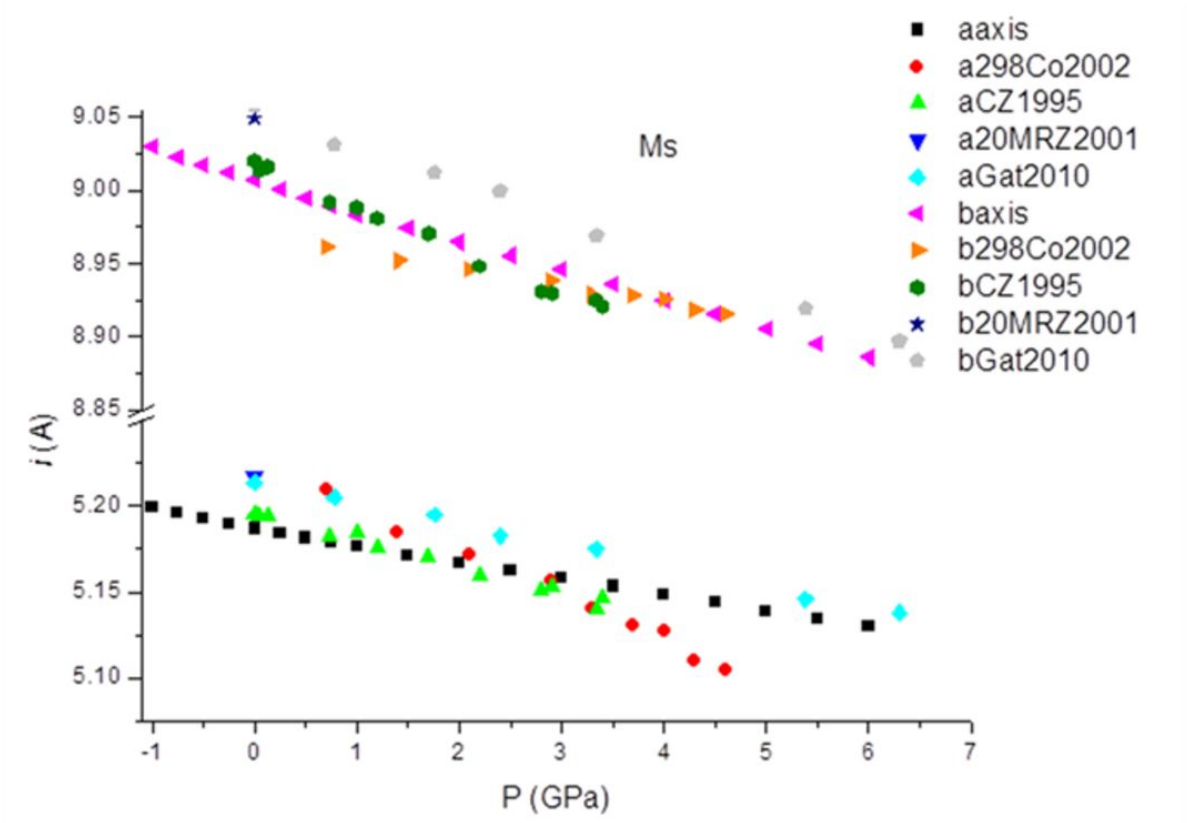

Figure 2a

This is a preprint, the final version is subject to change, of the American Mineralogist (MSA)
Cite as Authors (Year) Title. American Mineralogist, in press.
(DOI will not work until issue is live.) DOI: http://dx.doi.org/10.2138/am-2016-5407

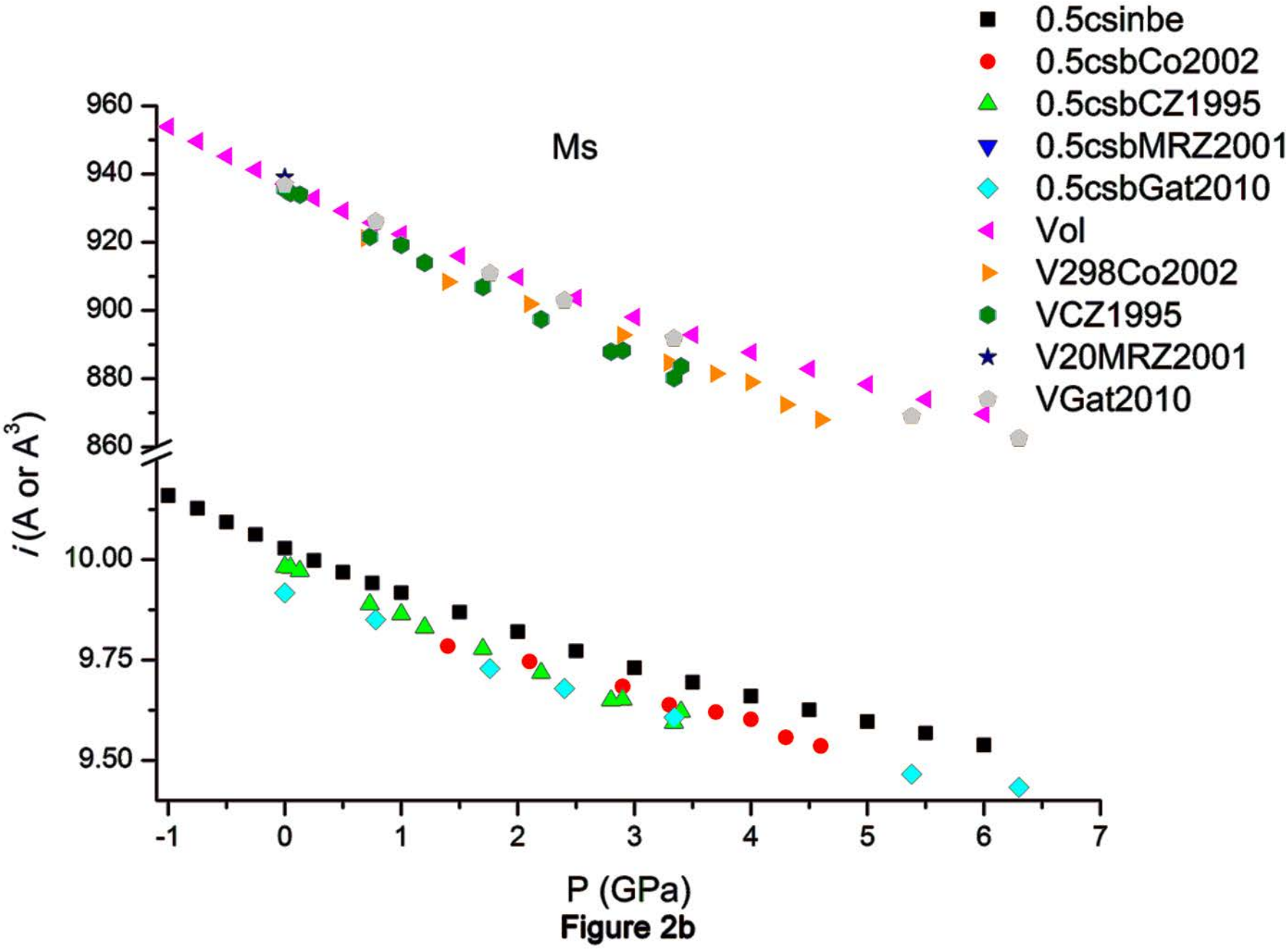

Figure 2b

This is a preprint, the final version is subject to change, of the American Mineralogist (MSA)
Cite as Authors (Year) Title. American Mineralogist, in press.
(DOI will not work until issue is live.) DOI: http://dx.doi.org/10.2138/am-2016-5407

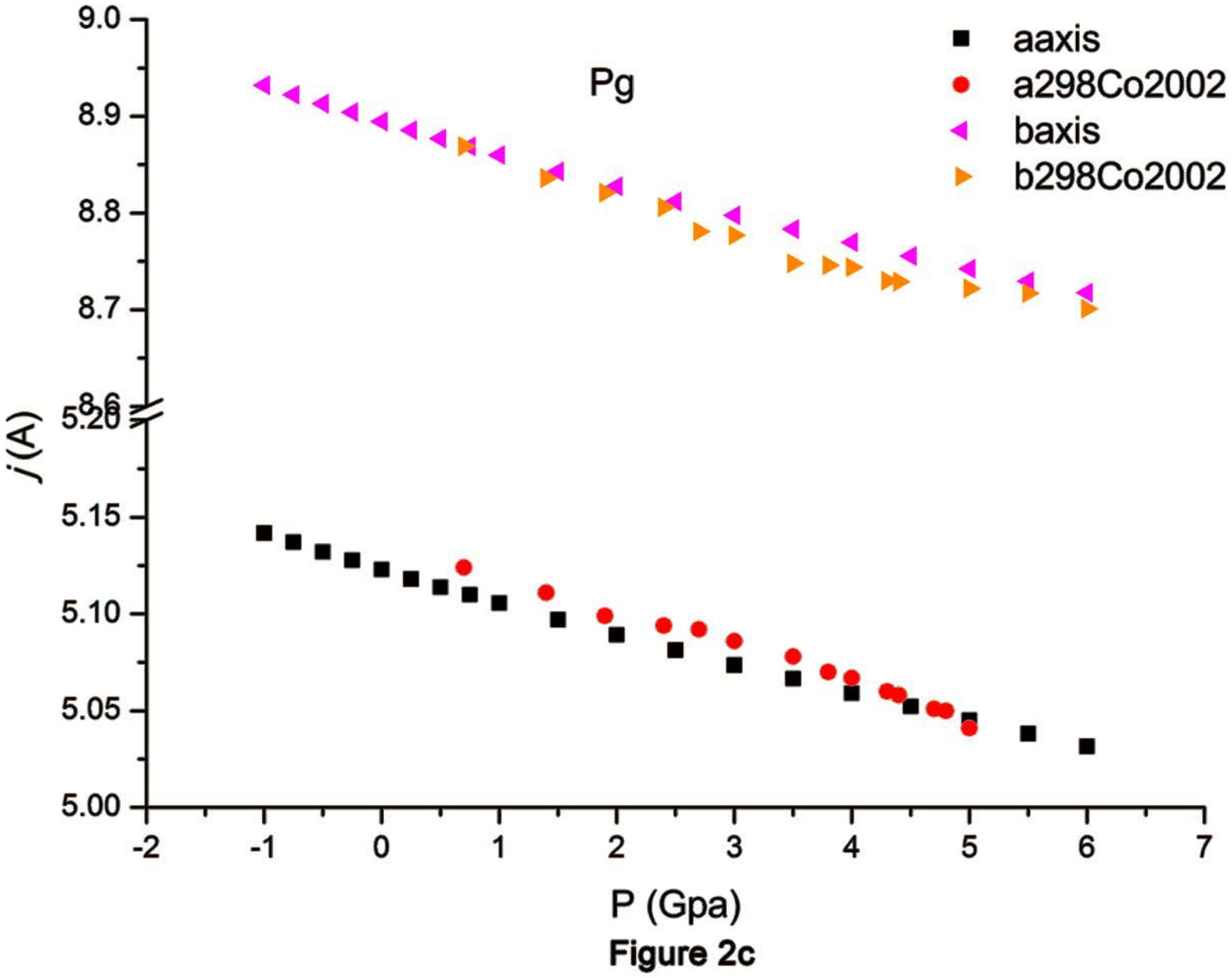

Figure 2c

This is a preprint, the final version is subject to change, of the American Mineralogist (MSA)
Cite as Authors (Year) Title. American Mineralogist, in press.
(DOI will not work until issue is live.) DOI: http://dx.doi.org/10.2138/am-2016-5407

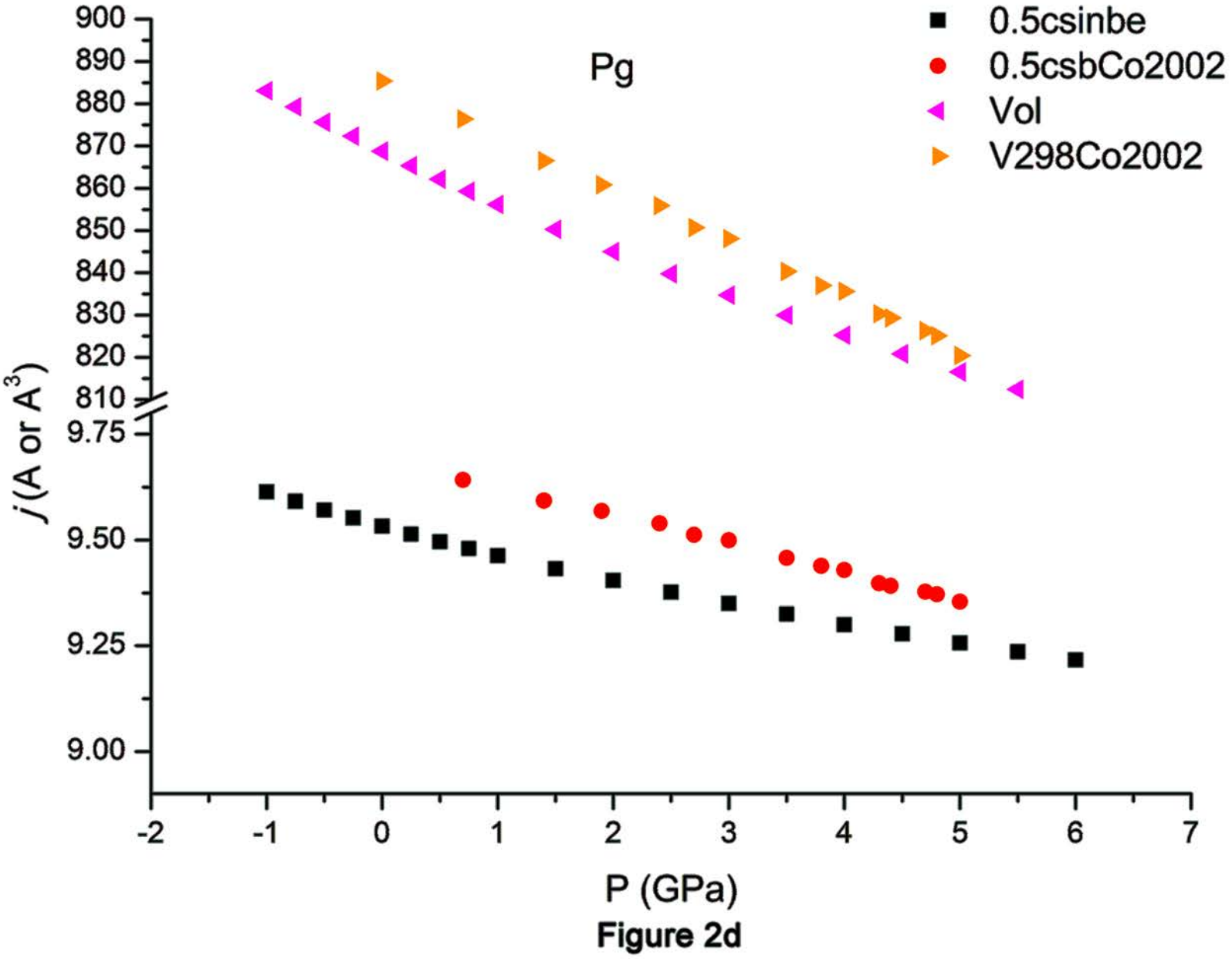

Figure 2d

This is a preprint, the final version is subject to change, of the American Mineralogist (MSA)
Cite as Authors (Year) Title. American Mineralogist, in press.
(DOI will not work until issue is live.) DOI: http://dx.doi.org/10.2138/am-2016-5407

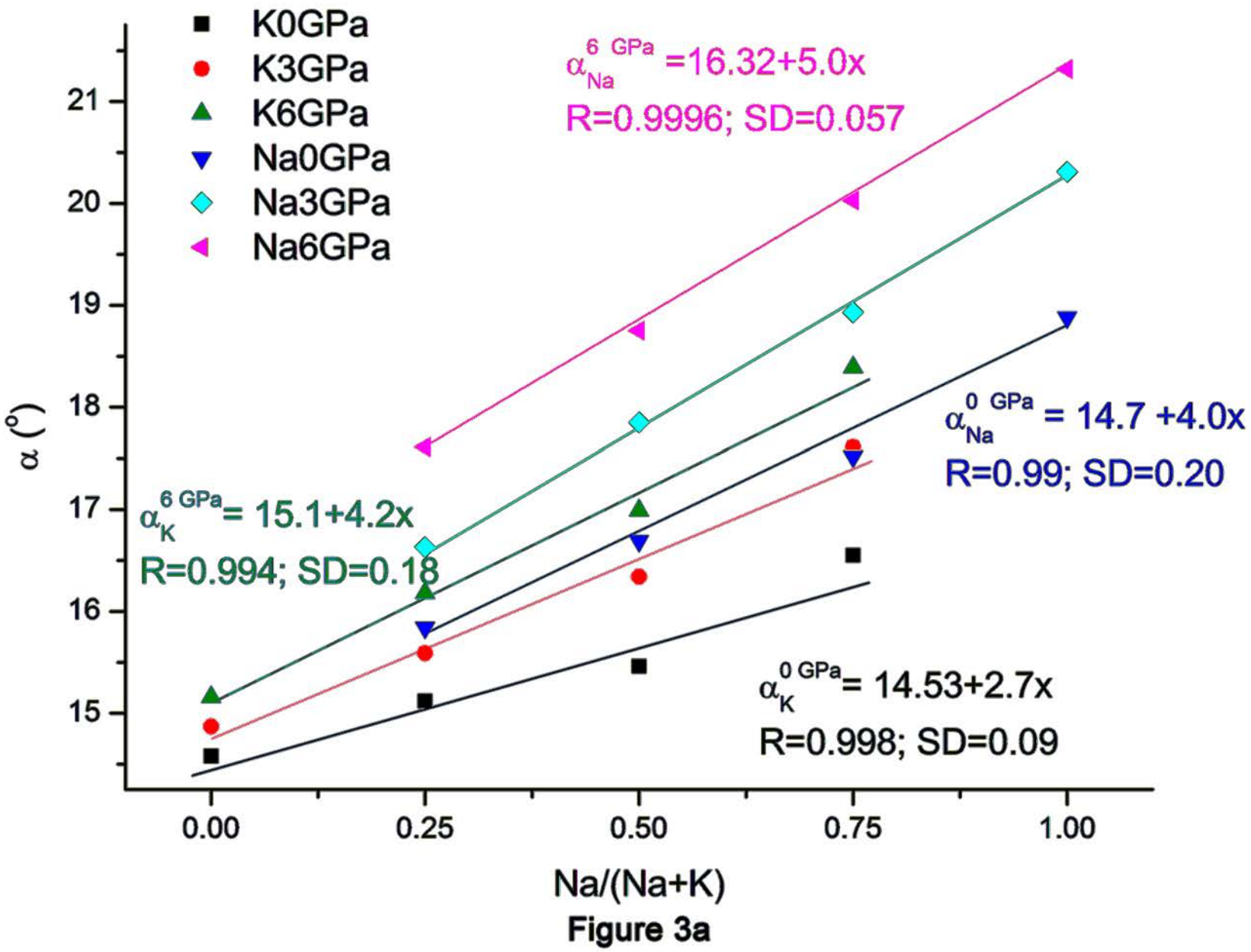

Figure 3a

This is a preprint, the final version is subject to change, of the American Mineralogist (MSA)
Cite as Authors (Year) Title. American Mineralogist, in press.
(DOI will not work until issue is live.) DOI: http://dx.doi.org/10.2138/am-2016-5407

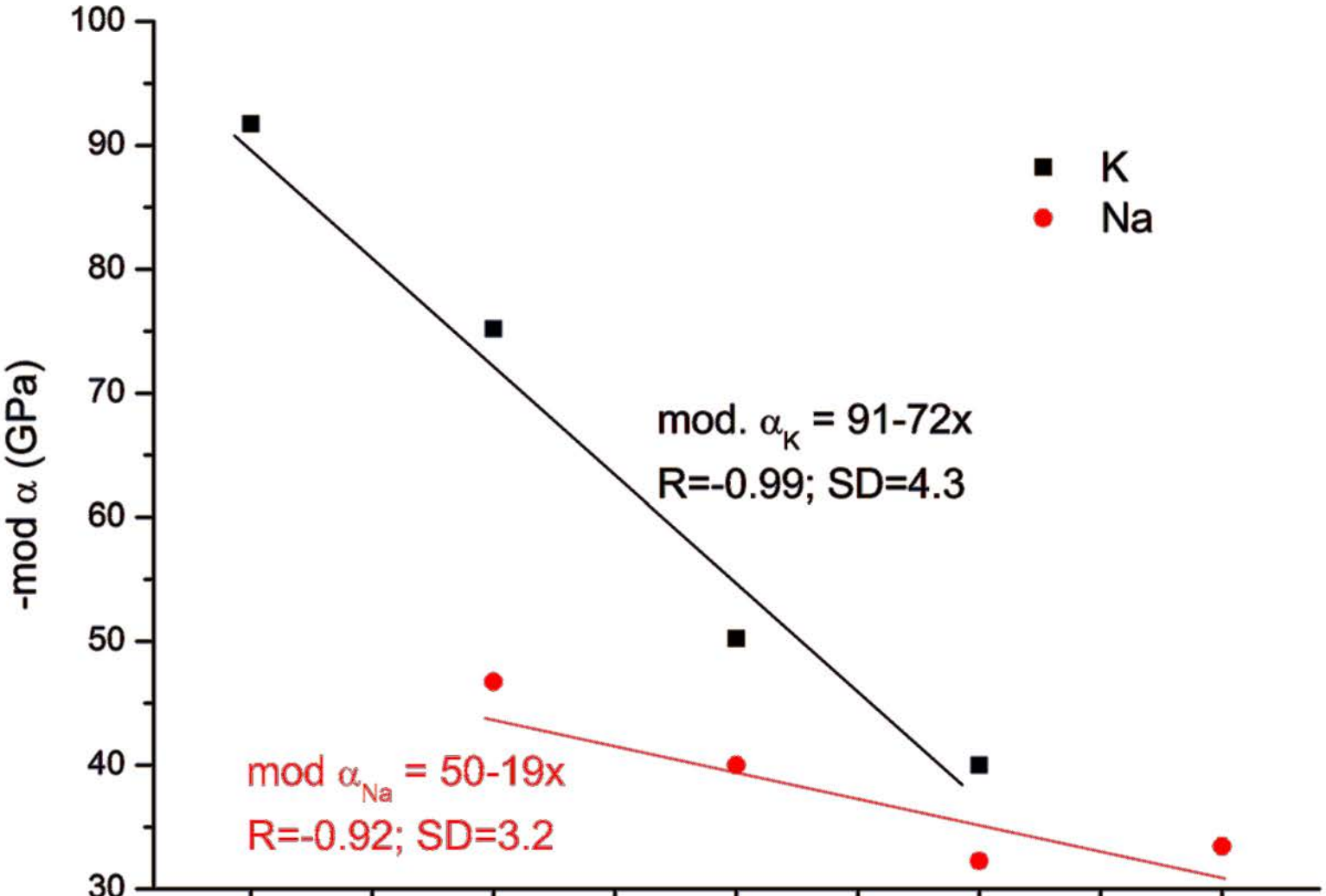

Figure 3b

This is a preprint, the final version is subject to change, of the American Mineralogist (MSA)
Cite as Authors (Year) Title. American Mineralogist, in press.
(DOI will not work until issue is live.) DOI: http://dx.doi.org/10.2138/am-2016-5407

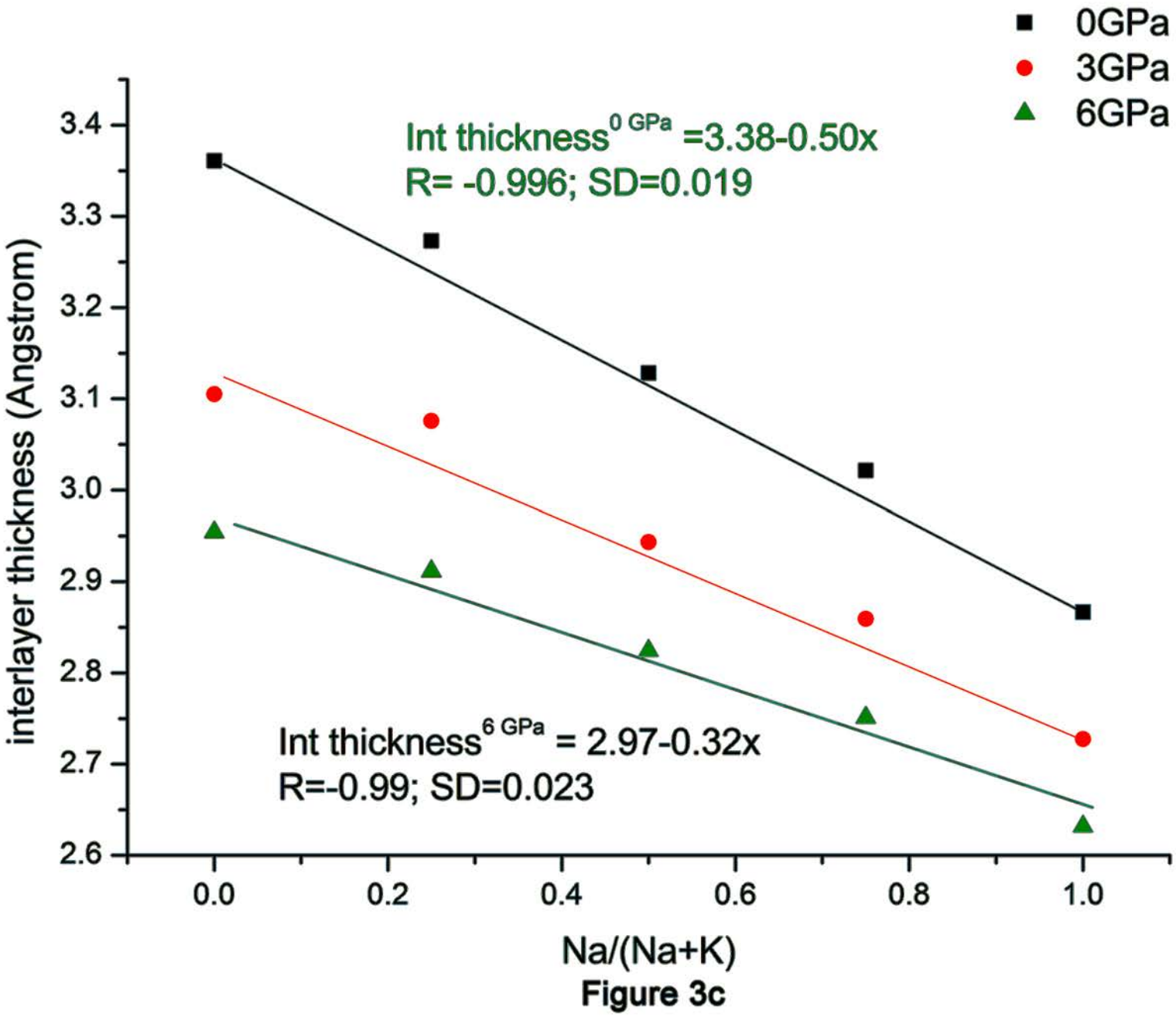

Figure 3c

This is a preprint, the final version is subject to change, of the American Mineralogist (MSA)
Cite as Authors (Year) Title. American Mineralogist, in press.
(DOI will not work until issue is live.) DOI: http://dx.doi.org/10.2138/am-2016-5407

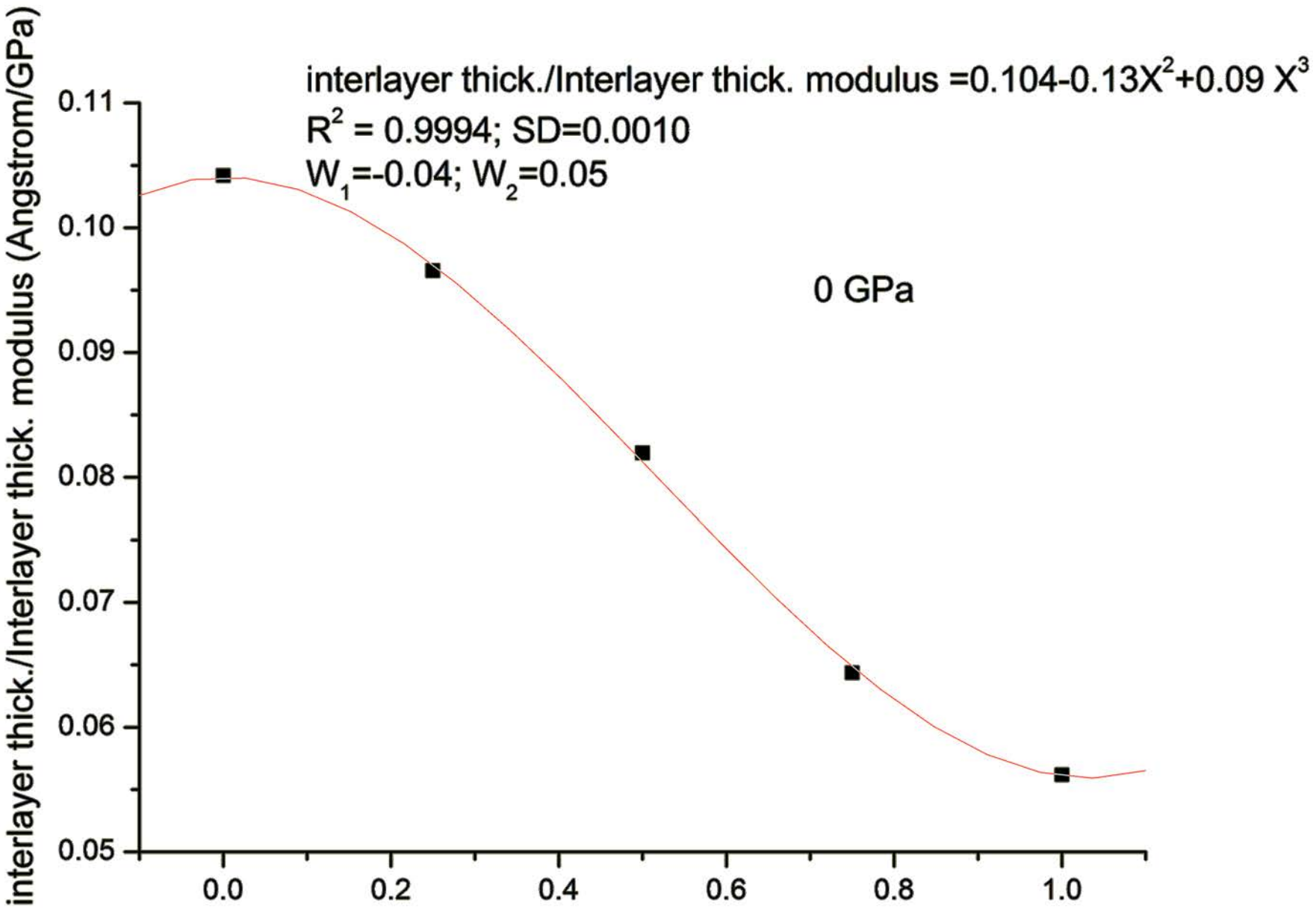

Figure 3d

This is a preprint, the final version is subject to change, of the American Mineralogist (MSA)
Cite as Authors (Year) Title. American Mineralogist, in press.
(DOI will not work until issue is live.) DOI: http://dx.doi.org/10.2138/am-2016-5407

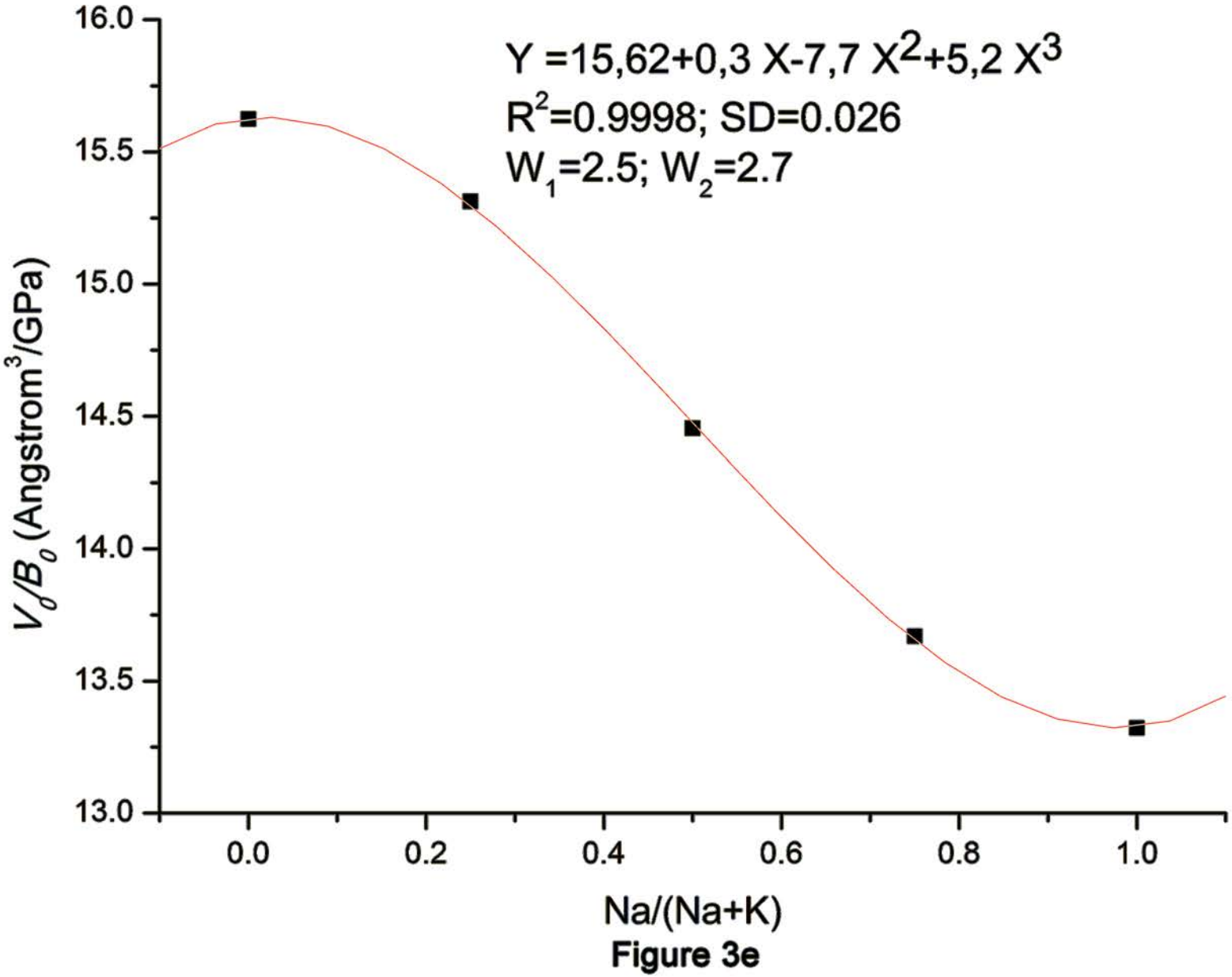

Figure 3e

This is a preprint, the final version is subject to change, of the American Mineralogist (MSA)
Cite as Authors (Year) Title. American Mineralogist, in press.
(DOI will not work until issue is live.) DOI: http://dx.doi.org/10.2138/am-2016-5407

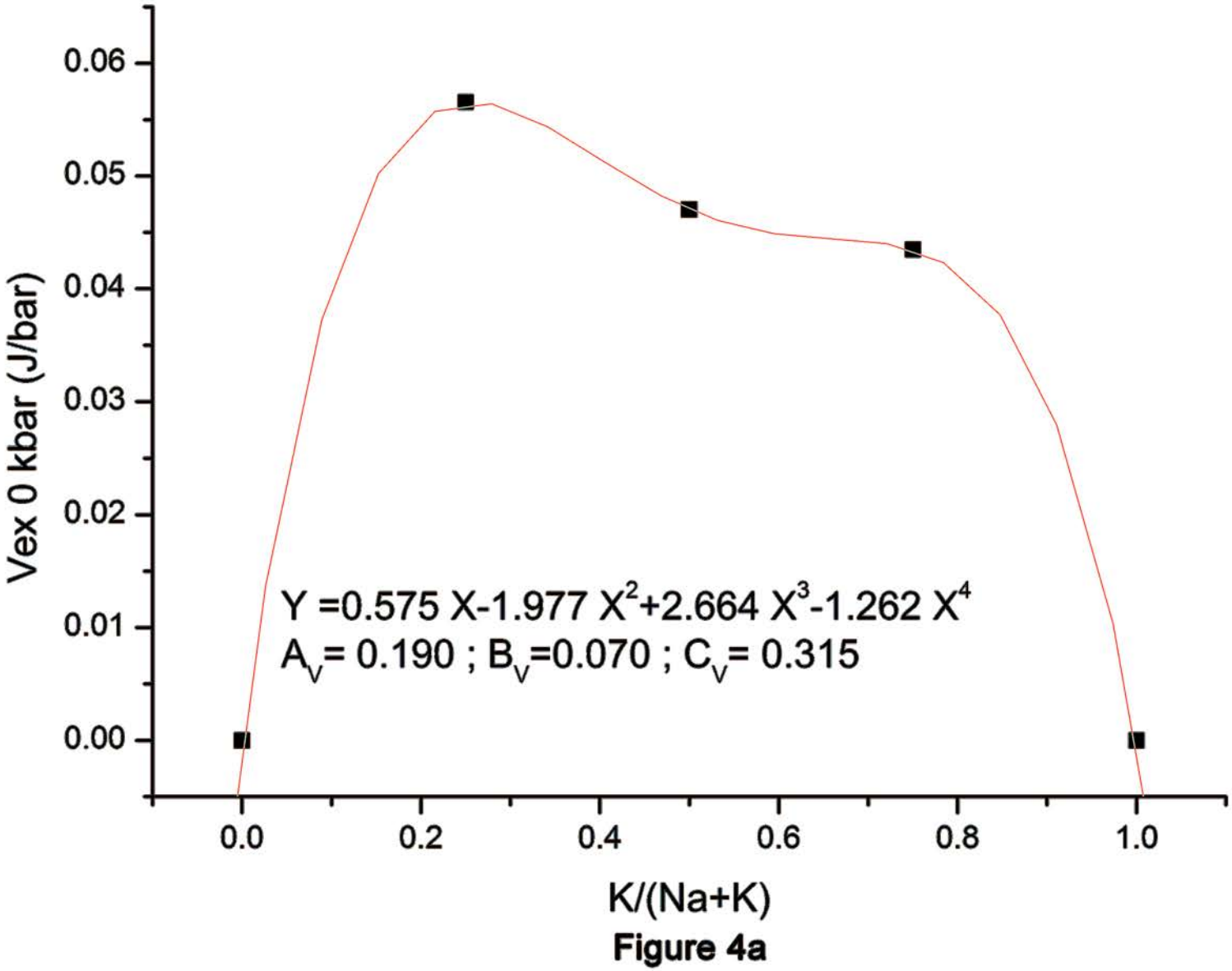

Figure 4a

This is a preprint, the final version is subject to change, of the American Mineralogist (MSA)
Cite as Authors (Year) Title. American Mineralogist, in press.
(DOI will not work until issue is live.) DOI: http://dx.doi.org/10.2138/am-2016-5407

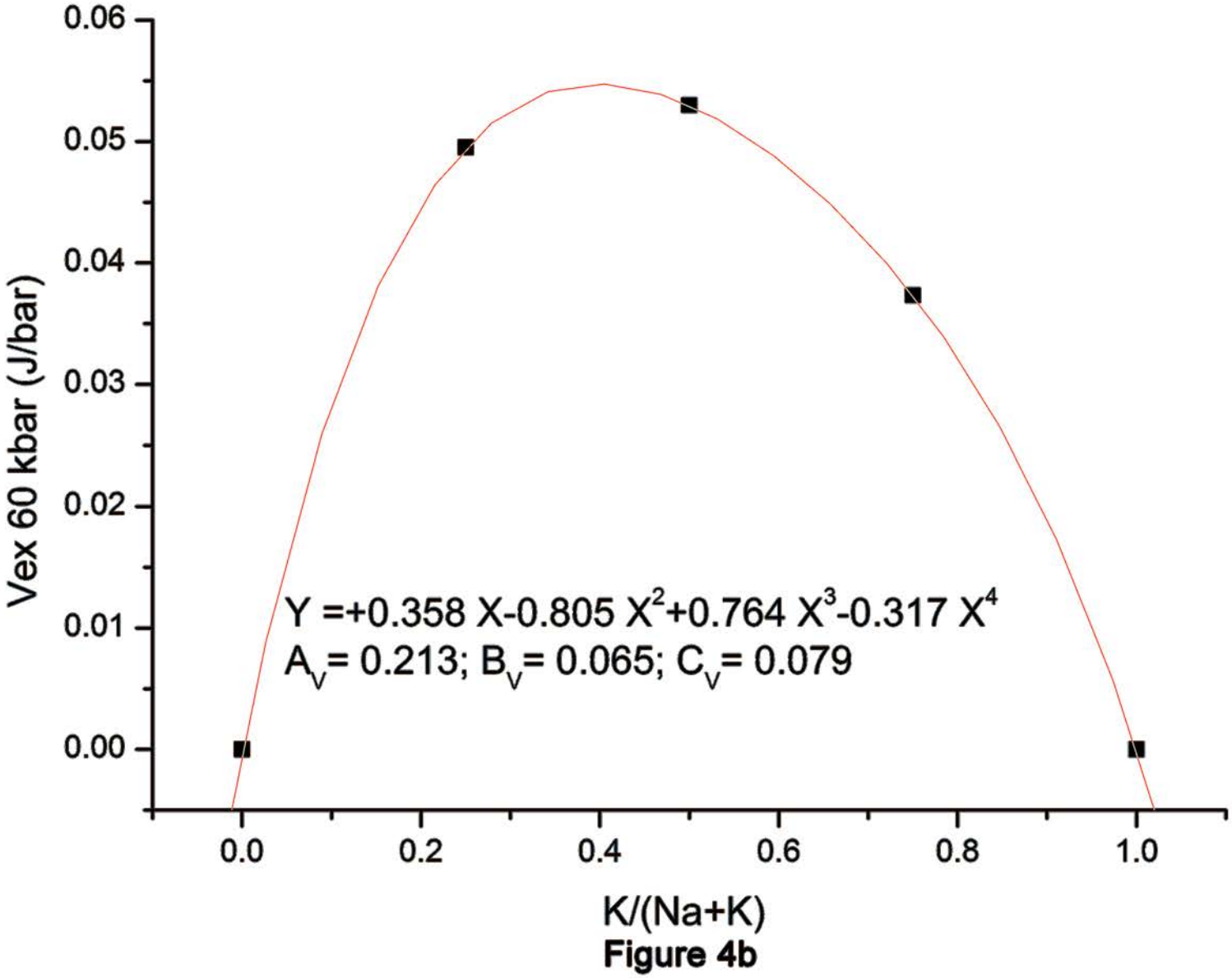

Figure 4b

This is a preprint, the final version is subject to change, of the American Mineralogist (MSA)
Cite as Authors (Year) Title. American Mineralogist, in press.
(DOI will not work until issue is live.) DOI: http://dx.doi.org/10.2138/am-2016-5407

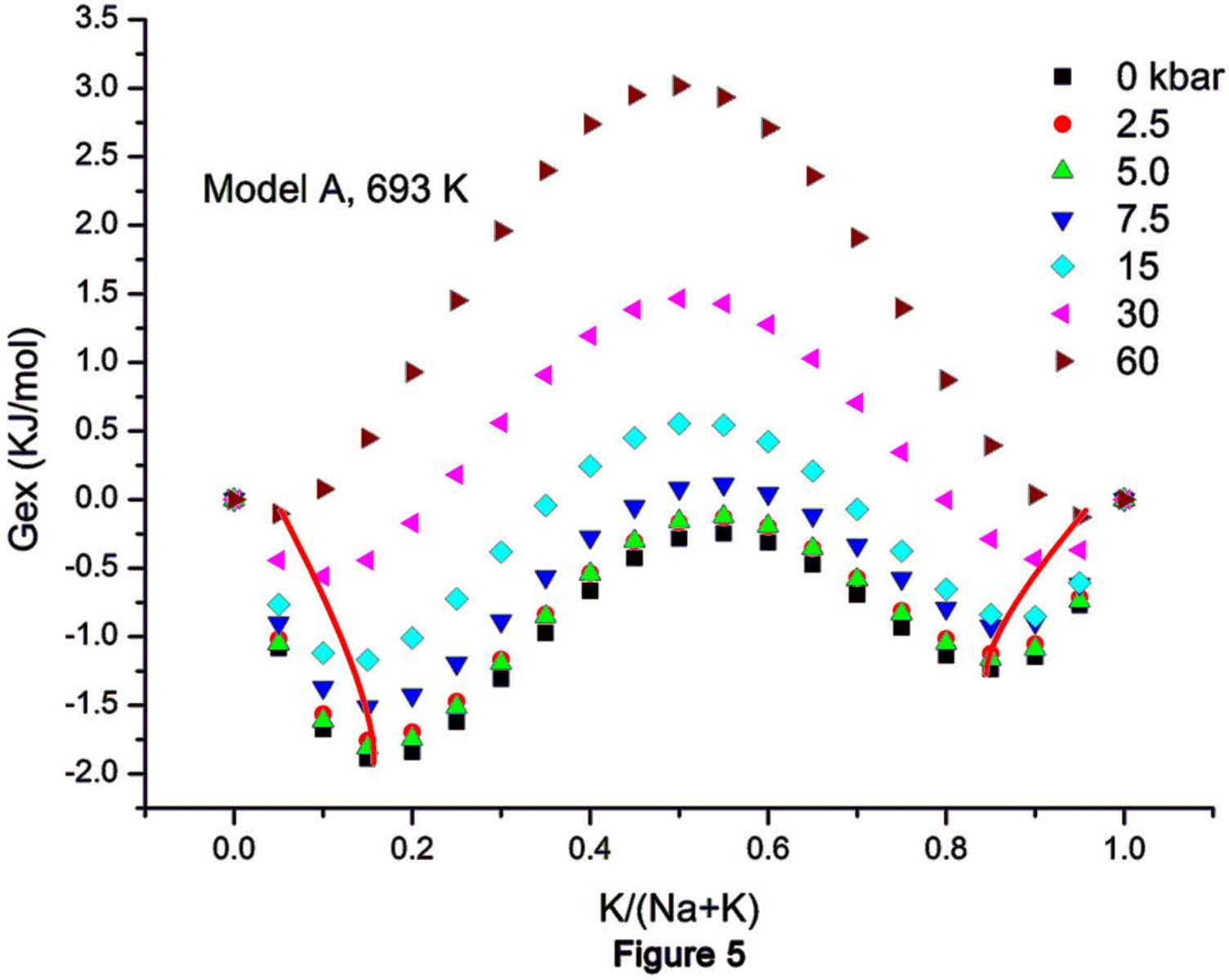

Figure 5